CHAPTER 4

Synthesis and characterization of 'piano-stool' type mixed ligand Ruthenium(II)- arene complexes.

Half-sandwich 'piano-stool' type organometallic ruthenium (II) arene compounds of the general structural formula [Ru(η^6-*p-cym*)(*L*)Cl] (*p-cym* = *p*-cymene $MeC_6H_4Pr^i$; *L* = N, O and O, O donor ligands discussed in chapter-2 i.e. Inh 1-4, FcA 1-4, Isa 1-4, Stb 1-4, Flq 1-3) have been synthesized and characterized by means of ESI mass spectrometry, NMR, FTIR and UV-Vis spectroscopy. These organometallic complexes were found to be pseudo-octahedral in geometry with three coordination sites taken up by the arene ligand (resonating structure) forming very stable arene-Ru bond that stabilizes ruthenium in its +2 state, while the remaining three sites are taken up by labile chloride ligands (which can be easily aquated) and a bidentate ligand.

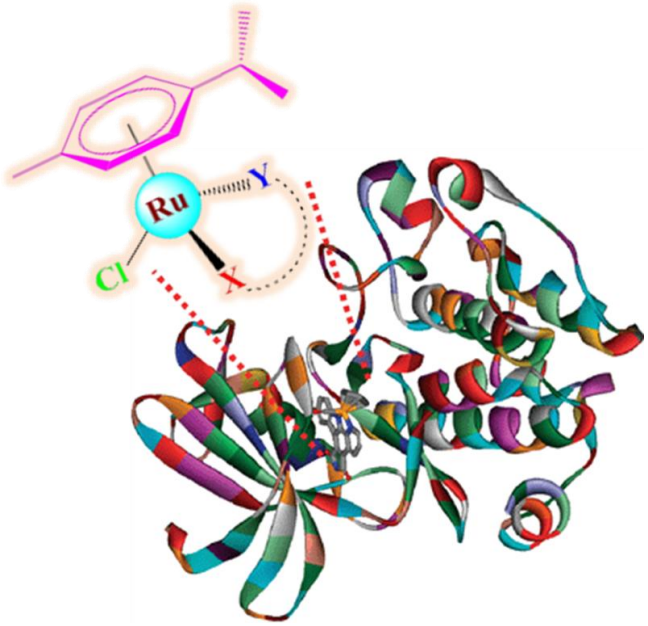

4.1 Introduction to Ruthenium(II)-arene complexes:

4.1.1 An account of organometallic Ru(II)-arene complexes with medicinal applications:

❖ **Organometallic chemistry, biology and medicine:**

In 1985, the term 'bioorganometallic chemistry' was introduced by Gérard Jaouen to describe any compound with a metal-carbon bond and a biological function, whether naturally occurring or synthetic [1]. In nature organometallic compounds are relatively rare or transient, perhaps best illustrated by the pioneering research on vitamin B_{12} [2], but there are many unnatural examples dominated by chemical pollutants - toxic and unstable compounds that can cause severe health problems [3]. Despite the reputation of organometallics as toxic pollutants, it is becoming increasingly evident that these compounds have unique properties that can be exploited in medicine. Organometallic compounds have potential applications in the treatments of cancer, microbial, viral and parasitic diseases and even exhibit cardioprotective effects [4]. Furthermore, organometallic compounds have certain properties that make them attractive in medicinal chemistry, such as their wide and diverse structural types, varied ligand bonding modes, and redox properties. To some extent, they exhibit properties intermediate between clinically proven coordination compounds and organic molecules. Consequently, organometallics comprise a stable scaffold or reactive center that can be fine tuned to facilitate the formulation stages of clinical trials and subsequent drug optimization and rational drug design processes. Traditionally, anticancer drug screening programs with coordination or organometallic complexes are based on selecting compounds with a high level of genotoxicity and cytotoxicity *in vitro*; however, many of these compounds subsequently fail to enter clinical trials because of stability and general toxicity issues. Recently, complexes that failed *in vitro* screening methods have been demonstrated to have promising *in vivo* activity. Notable examples of such complexes include the coordination complexes indazolium [*trans*-tetrachlorobis(1*H*-indazole)ruthenate(III)], KP1019 [5,6], and imidazolium trans-[tetrachloro-(S-dimethyl-sulfoxide)(1*H*-imidazole)ruthenate(III)], NAMI-A [7,8] (both now in phase II clinical trials) (discussed in *Ch. 1*)

Since arenes are known to stabilise ruthenium in its 2+ oxidation state, investigations have been done into the potential of Ru(II) arene complexes as anticancer agents and their associated aqueous chemistry. It is found that ''half-sandwich'' Ru(II) mono-arene complexes often possess good aqueous solubility (an advantage for clinical use) and that the arene ligand is relatively inert towards displacement under physiological conditions. There is a delicate balance between electron donation from the arene into the empty Ru

4d orbitals and back-donation from the filled $4d^6$ orbitals into vacant arene orbitals. This is influenced by the donor–acceptor power of the arene (e.g. hexamethylbenzene as a strong donor, in contrast to biphenyl which may act as acceptor) and by the other ligands on Ru(II) which can influence the availability of the Ru $4d^6$ electrons, e.g. presence of strong π-acceptor chelating ligands such as bipyridine and azopyridine [9], or donor strength of mondentate ligands (e.g. iodide vs. chloride) [10]. In this context, very recently, attention has been focused on organometallic Ru(II) arene complexes and their anticancer activities have been studied by varying the arene, substituent ligand and leaving group [11]. These 'piano-stool' frameworks provide a handle for optimizing the design of drugs in terms of pharmacological properties and reducing the side effects.

❖ **Structure of Ru(II) arene complex:**

A typical structure of a half-sandwich 'piano-stool' [Ru(η^6-arene) (X)(YZ)] complex is shown in *Fig. 4.1*, where the arene forms the seat of the piano stool and the ligands resemble the legs. Linking the ligands Y and Z to form a bidentate chelating ligand (L) seems to be advantageous for anticancer activity. The structure of Ru(II) half-sandwich complexes allows for variations of the three main building blocks, the monodentate ligand X, the bidentate ligand L and the arene, to fine-tune the pharmacological properties of these complexes. The chelating ligand can help to control the stability and ligand-exchange kinetics of these complexes. The nature of the arene can help to influence cell uptake and interactions with potential targets. The leaving group, which typically is chloride and occupies the biomolecule binding site on the metal centre, can be of importance to control the timing of activation of these complexes [12].

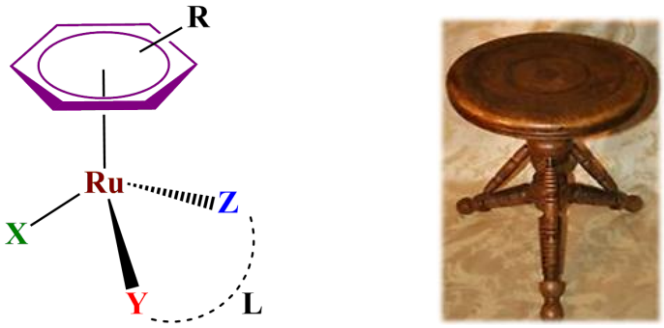

Fig. 4.1: *Typical structure of the Ru(II) half-sandwich complex with the general formula [Ru(η^6-arene) (X)(YZ)] showing the resemblance with a 'piano-stool'*

❖ **Pioneers of Ru(II)-arene chemistry:**

The field of antitumoural and antimetastatic arene ruthenium complexes was pioneered by P.J.Dyson and by P.J.Sadler, [13,14] after the notion of using arene ruthenium compounds as anticancer agents had first been introduced by Tocher *et al.* in

1992, who had observed a cytotoxicity enhancement by coordinating the anticancer agent metronidazole [1-β-(hydroxyethyl)-2-methyl-5-nitro-imidazole] to a benzene ruthenium dichloro fragment [15]. Initially, the prototype arene ruthenium(II) complexes evaluated for anticancer properties in 2001 were (η^6-*p*-$MeC_6H_4Pr^i$)Ru(*P*-pta)Cl_2 (*pta = 1,3,5-triaza-7-phospha-tricyclo-[3.3.1.1]decane*), termed RAPTA-C, from Dyson's laboratory, [16] and [(η^6-C_6H_5Ph)Ru(*N*,*N*-en)Cl]$^+$ (*en = 1,2-ethylenediamine*) as hexafluorophosphate salt as well as some analogues from Sadler's laboratory (*Fig. 4.2*) [17]. Although RAPTA-C exhibits only a low activity *in vitro*, it is very active *in vivo*, where it inhibits lung metastases in mice; like NAMI-A, RAPTA-C is also an antimetastatic agent [13].

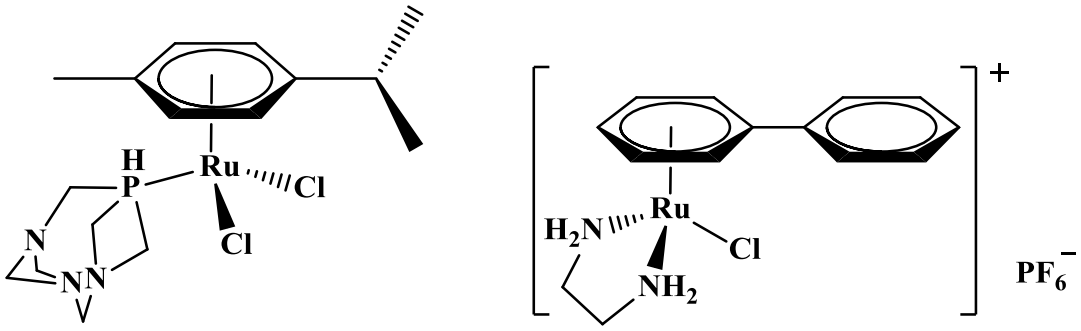

RAPTA-C **RM175**

(P.J.Dyson *et. al.)* **(P.J.Sadler *et. al.*)**

Fig. 4.2: *Prototype anticancer arene ruthenium complexes reported by Dyson and by Sadler.*

❖ **SAR of Ru(II) arene complexes:**

From the confluence of the chemical, biochemical and biological studies on these two main classes of compounds the valuable pharmacological properties of the organometallic ruthenium(II)-arene unit emerged [18]. These properties have been depicted in *Fig. 4.3* and may be summarized as follows:

- The ruthenium(II) ion is a viable metal ion for biological applications when coordinated to an arene ligand. Since it was postulated that Ru(III) complexes are prodrugs, activated only in cancer cells by reduction to Ru(II), there was a concern that Ru(II) complexes would display systemic toxicity and this does not appear to be the case. The stability of the ruthenium-arene bond allows compounds to be modified in a rational way so that functionality, e.g. biologically active groups, can be introduced in a relatively facile manner. Thus, the ruthenium-arene fragment represents an excellent scaffold on which to build functional organic segments for targeted chemotherapy.
- The arene ligand provides a bulky hydrophobic surface that helps to endow the compounds with a degree of selectivity with respect to binding biomolecular targets.

It should be noted, however, that while increasing hydrophobicity tends to increase cytotoxicity, this does not necessarily lead to improved selectivity, i.e. cancer versus healthy cells.

- Hydrolysis of the Ru-Cl bond allows direct coordination to biomolecular targets and an active role of a toxic heavy metal such as ruthenium is important. The rate of reaction with biomolecular targets can be modulated by using other (labile) ligands in place of the chlorides.
- Ancillary ligands can also be used to modulate the pharmacological properties of ruthenium(II)-arene compounds.

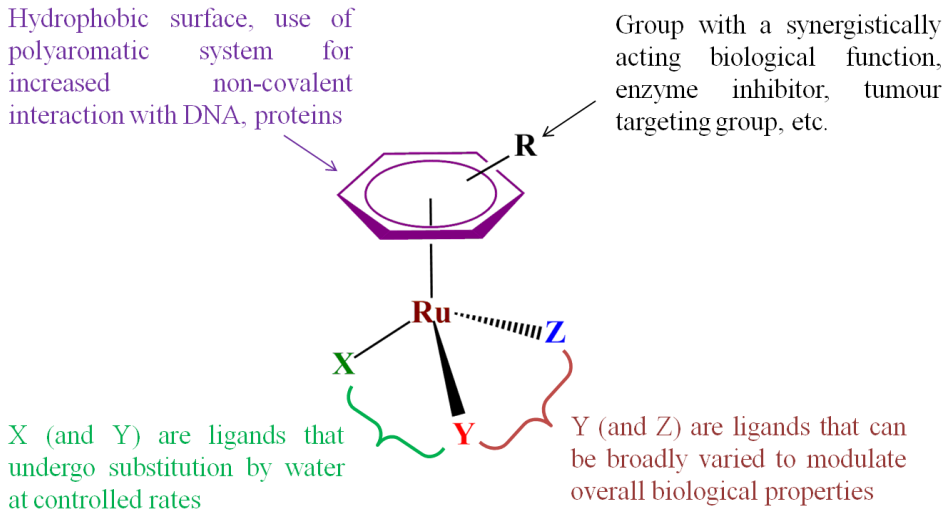

Fig. 4.3: *Generic structure of ruthenium(II)-arene compounds illustrating the ways in which the central structural motif can be modified to tune its pharmacological properties. X, Y and Z can be mono, bi or tri-dentate ligands.*

4.1.2 Past, present and future of Ru(II)-arene complexes:

When Bennett and co-workers published the facile synthesis of some ruthenium(II)arene dimers bridged by chlorido ligands in 1974 [19], it is unlikely that they would have anticipated the profound impact their work would have in many different domains. A plethora of compounds have been derived from these truly versatile starting materials that have found extensive, important applications in catalysis, remarkable applications as synthons in supramolecular chemistry to afford sensors, and compounds with intriguing biological properties, some with potentially valuable clinical uses. Very recently, it has been shown that these dimer precursors can be prepared in minutes using microwave dielectric heating, which makes them more easily accessible and likely further broadens their application [20]. From a chemical perspective, the comparatively robust nature of the organometallic scaffold present in ruthenium-arene compounds presents an ideal template for rational drug design [21]. The study of the biological properties of

ruthenium(II)-arene complexes is certainly not as extensive as that of their catalytic properties, and yet, growth in the field has been remarkable over the last few years. Further mechanistic insight is also required to help design strategies in the future. The rich selection of organometallic ruthenium(II)-arene compounds with a multitude of innovative modes of action has added new flavour to the field of metal-based anticancer agents and holds great promise for future drug development.

Following the insights into how organometallic ruthenium complexes could work towards the finding of new anticancer drugs, half-sandwich 'piano-stool' type organometallic ruthenium (II) arene compounds of the general structural formula [Ru(η^6-*p-cym*)(*L*)Cl] (*p-cym* = *p*-cymene $MeC_6H_4Pr^i$; *L* = N, O and O, O donor ligands) have been synthesized and characterized by means of various spectroscopic techniques. These complexes were then evaluated upon for their biological activities employing various assays.

4.2 General synthesis of [Ru(η^6-p-cym)(L)Cl] complexes:

4.2.1 Materials and instrumentation:

All the chemicals and solvents used for the synthesis and characterization of **[Ru(η^6-*p*-cym)(L)Cl]** complexes are of analytical grade and were used as purchased. The precursor [Ru(η^6-*p*-cymene)Cl_2]$_2$ was prepared according to the procedure sited in literature [19,22]. α-terpinene was purchased from Sigma-Aldrich. $RuCl_3$. $3H_2O$ was purchased from Hi-media, Mumbai, India.

ESI-Mass spectra, IR, UV-Vis spectra and elemental analyses were recorded on the same instrument models as mentioned previously in *Sec. 3.2.1*. ^{1}H NMR spectra were recorded on Bruker 400 MHz NMR Spectrophotometer.

4.2.2 General synthetic scheme:

Complexes of general formula, [Ru(η^6-*p*-cymene)(L)Cl] were prepared by a typical μ-chlorido-bridge splitting reaction of [Ru(η^6-*p*-cymene)Cl_2]$_2$. To a solution of [Ru(η^6-*p*-cymene)Cl_2]$_2$ (in 2.5 ml CH_2Cl_2), the synthesized ligand **L** (in 2.5 ml methanol) was added on stirring in 1:2 mole ratio respectively. The reaction mixture was left on stirring for overnight (20-24 h) at room temperature and then for slow evaporation. The resultant reddish brown crystalline solid was then filtered, washed with pet ether and CH_2Cl_2 and dried in oven at 40°C for 1 h. The complexes so obtained were recrystallized from dichloromethane and ether which resulted in reddish brown crystals but not of the single crystal quality. *Fig. 4.4* shows the general synthetic route for the preparation of **[Ru(η^6-*p*-cym)(L)Cl]** complexes.

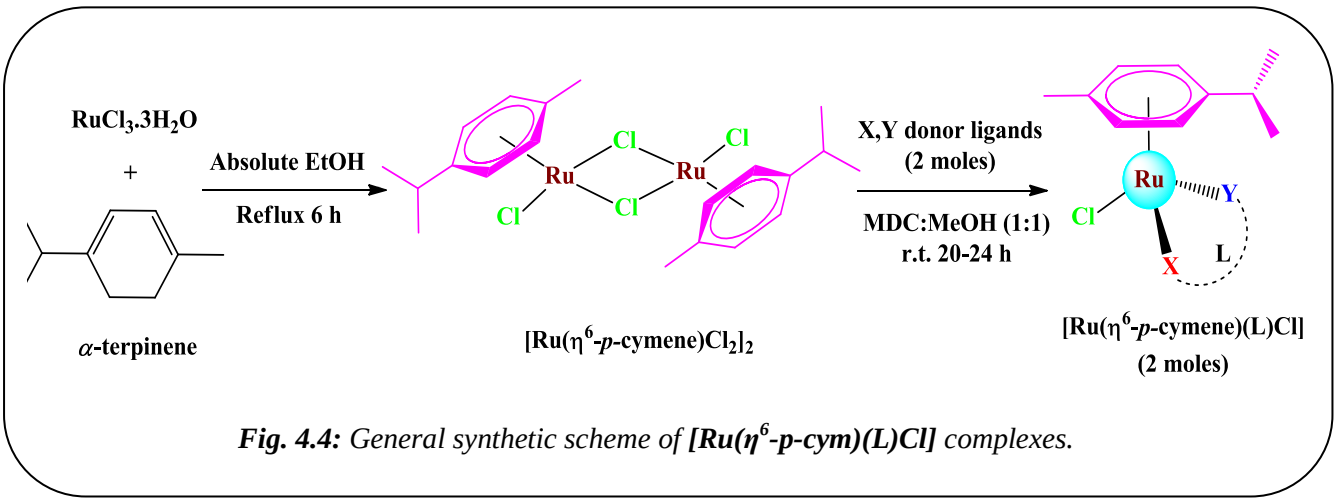

Fig. 4.4: *General synthetic scheme of* ***[Ru(η^6-p-cym)(L)Cl]*** *complexes.*

Where, **L** stands for the synthesized ligands (discussed in *Ch.2*)

Table 4.1: *List of the different ligand series used in the synthesis of [Ru(η^6-p-cym)(L)Cl] complexes along with their coordinating sites to the Ru(II) centre.*

L = Ligands	*Ligand codes*	*Complex codes*	*X*	*Y*
Isoniazid derivatives	**Inh 1-4**	**RAInh 1-4**	N	O
Ferrocenyl derivatives	**FcA 1-4**	**RAFcA 1-4**	N	O
Stilbene derivatives	**Stb 1-4**	**RAStb 1-4**	Cl	N
Isatin derivatives	**Isa 1-4**	**RAIsa 1-4**	N	O*
Fluoroquinolones	**Flq 1-3**	**RAFlq 1-3**	O	O

***Note:** in case of **RAIsa-4** Y=S*

The composition and structures of all the **[Ru(η^6-*p*-cym)(L)Cl]** complexes have been confirmed by ESI Mass spectrometry, NMR, FTIR, UV-Vis spectroscopy and elemental analysis. The analytical data are consistent with the proposed compositions and their molecular formulae.

4.3 [Ru(η^6-p-cym)(Inh 1-4)Cl] complexes: (RAInh 1-4)

4.3.1 Synthesis and characterization:

[Ru(η^6-p-cym)(Inh-1)Cl] **(RAInh-1)**:

RAInh-1 was synthesized by reaction of [Ru(η^6-*p*-cymene)Cl_2]$_2$ (0.049 mmol, 30.0 mg) and ligand **Inh-1** (0.098 mmol, 22.1 mg). Soluble in almost all organic solvents like DMSO, MeOH, CH_2Cl_2. Yield: 75.7%; Molecular Weight 494.98 g/mole; Molecular Formula $C_{23}H_{24}ClN_3ORu$; Anal. Found: C, 53.34; H, 5.30; N, 7.52. Calc.: C, 55.81; H, 4.89; N, 8.49. ESI-MS *m/z*: 495.9 (M^++1), 460 (M^+-Cl); δ_H (400 MHz, DMSO-d_6): 8.81 (d, 2H, pyridyl α-H), 8.51 (s, 1H, N=CH), 7.89 (d, 2H, pyridyl β-H), 7.76 (d, 2H, Ar-H), 7.48-7.46 (m, 3H, Ar-H), 5.82-5.77 (m, 4H, *p*-cym Ar-H), 2.81 (q, 1H, *p*-cym-*iso*-prop-CH), 2.08 (s, 3H, *p*-cym Ar-CH_3), 1.19 (d, 6H, *p*-cym-*iso*-prop-$(CH_3)_2$); FTIR (KBr/ cm^{-1}): $\nu_{(Ar)C-H}$ 3051, $\nu_{C=N}$ 1678, ν_{C-O} 1148.

[Ru(η^6-p-cym)(Inh-2)Cl] **(RAInh-2)**:

RAInh-2 was synthesized by reaction of [Ru(η^6-*p*-cymene)Cl_2]$_2$ (0.049 mmol, 30.0 mg) and ligand **Inh-2** (0.098 mmol, 23.6 mg). Soluble in almost all organic solvents like DMSO, MeOH, CH_2Cl_2. Yield: 71.4%; Molecular Weight 510.98 g/mole; Molecular Formula $C_{23}H_{24}ClN_3O_2Ru$; Anal. Found: C, 51.93; H, 4.52; N, 7.09. Calc.: C, 54.06; H, 4.73; N, 8.22. ESI-MS *m/z*: 512.4 (M^++1), 475.9 (M^+-Cl); δ_H (400 MHz, DMSO-d_6):

12.55 (s, 1H, OH), 8.90 (d, 2H, pyridyl α-H), 8.76 (s, 1H, N=CH), 8.05 (d, 2H, pyridyl β-H), 7.62 (d, 1H, Ar-H), 7.32 (t, 1H, Ar-H), 6.97-6.93 (m, 2H, Ar-H), 5.82-5.77 (m, 4H, *p*-cym Ar-H), 2.81 (q, 1H, *p*-cym-*iso*-prop-CH), 2.08 (s, 3H, *p*-cym Ar-CH_3), 1.19 (d, 6H, *p*-cym-*iso*-prop-$(CH_3)_2$); FTIR (KBr/ cm^{-1}): $\nu_{(Ar)C-H}$ 2987, $\nu_{C=N}$ 1683, ν_{C-O} 1151.

[Ru(η^6-p-cym)(Inh-3)Cl] **(RAInh-3)**:

RAInh-3 was synthesized by reaction of $[Ru(\eta^6\text{-}p\text{-cymene})Cl_2]_2$ (0.049 mmol, 30.0 mg) and ligand **Inh-3** (0.098 mmol, 26.6 mg). Soluble in almost all organic solvents like DMSO, MeOH, CH_2Cl_2. Yield: 68.3%; Molecular Weight 541.00 g/mole; Molecular Formula $C_{24}H_{26}ClN_3O_3Ru$; Anal. Found: C, 52.15; H, 4.01; N, 6.23. Calc.: C, 53.28; H, 4.84; N, 7.77. ESI-MS *m/z*: 541.3 (M^+), 505.9 (M^+-Cl); δ_H (400 MHz, DMSO-d_6): 12.20 (s, 1H, OH), 8.87 (d, 2H, pyridyl α-H), 8.44 (s, 1H, N=CH), 8.01 (d, 2H, pyridyl β-H), 7.32 (d, 1H, Ar-H), 7.12 (d, 1H, Ar-H), 6.88 (d, 1H, Ar-H), 5.82-5.77 (m, 4H, *p*-cym Ar-H), 3.83 (s, 3H, OCH_3), 2.81 (q, 1H, *p*-cym-*iso*-prop-CH), 2.07 (s, 3H, *p*-cym Ar-CH_3), 1.24 (d, 6H, *p*-cym-*iso*-prop-$(CH_3)_2$); FTIR (KBr/ cm^{-1}): $\nu_{(Ar)C-H}$ 2994, $\nu_{C=N}$ 1679, ν_{C-O} 1150.

[Ru(η^6-p-cym)(Inh-4)Cl] **(RAInh-4)**:

RAInh-4 was synthesized by reaction of $[Ru(\eta^6\text{-}p\text{-cymene})Cl_2]_2$ (0.049 mmol, 30.0 mg) and ligand **Inh-4** (0.098 mmol, 25.0 mg). Soluble in almost all organic solvents like DMSO, MeOH, CH_2Cl_2. Yield: 77.7%; Molecular Weight 525.01 g/mole; Molecular Formula $C_{24}H_{26}ClN_3O_2Ru$; Anal. Found: C, 53.00; H, 4.60; N, 6.19. Calc.: C, 54.91; H, 4.99; N, 8.00. ESI-MS *m/z*: 526.0 (M^++1), 490.0 (M^+-Cl); δ_H (400 MHz, DMSO-d_6): 8.84 (d, 2H, pyridyl α-H), 8.48 (s, 1H, N=CH), 7.99 (d, 2H, pyridyl β-H), 7.71 (d, 2H, Ar-H), 7.05 (d, 2H, Ar-H), 5.82-5.77 (m, 4H, *p*-cym Ar-H), 3.81 (s, 3H, OCH_3), 2.81 (q, 1H, *p*-cym-*iso*-prop-CH), 2.08 (s, 3H, *p*-cym Ar-CH_3), 1.19 (d, 6H, *p*-cym-*iso*-prop-$(CH_3)_2$); FTIR (KBr/ cm^{-1}): $\nu_{(Ar)C-H}$ 3051, $\nu_{C=N}$ 1660, ν_{C-O} 1171.

4.3.2 Results and discussion:

The IR spectra of complexes **RAInh 1-4** lack the strong secondary amide carbonyl absorption at 1680–1700 cm^{-1} that is typically seen in the spectra of the free ligands **Inh 1-4**. In all the complexes, the $\nu_{C=N}$ band is shifted to higher frequency between 1650 and 1680 cm^{-1} indicating coordination of the Schiff bases through the azomethine nitrogen [23]. The enolate structure of the coordinated ligand is supported by bands in the range of 1050-1170 cm^{-1} due to the enolic C-O stretching [24]. The N-H stretching bands in the range 3150–3250 cm^{-1} found in the IR spectra of **Inh 1-4** are completely lost in the

spectra of complexes which is also indicative of the enolization and deprotonation on coordination to the metal centre. Moreover the presence of weak to medium bands in the fingerprint regions 2900-3000 cm^{-1} owing to aromatic ν_{C-H} stretch and strong bands around 1430-1667 cm^{-1} due to the aromatic $\nu_{C=C}$ in plane vibrations is indicative of presence of *p*-cymene in the complex.

The electronic absorption spectra of the complexes (*Fig. 4.5*) show three major bands in the wavelength range 200-600 nm. The first band appearing within 200-250 nm region can be assigned to the intraligand $\pi \rightarrow \pi^*$ transition of the aromatic rings of the arene ligand (*p*-cymene) as well as the hydrazone ligand (Inh). The second band observed within 270-300 nm region can be assigned to the $n \rightarrow \pi^*$ transitions. Whereas the broad bands in the region 320-350 nm is observed as the third band owing to MLCT transitions. The λ_{max} values of all the transitions taking place in **RAInh 1-4** have been tabulated in *Table 4.2*.

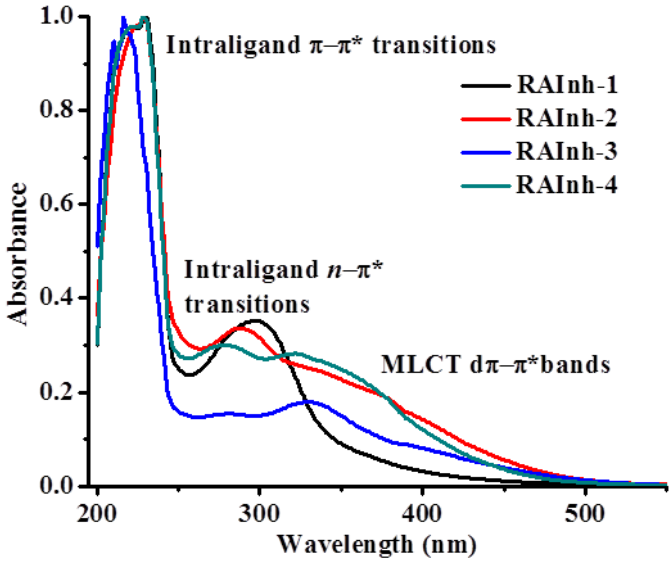

Fig. 4.5: *UV-vis. spectra of complexes* ***RAInh 1-4*** *recorded in DMSO with path length 1 cm.*

Table 4.2: *UV-Vis. peak assignments of* ***RAInh 1-4***

Compound	*Intra-ligand transitions (nm)*		*MLCT dπ-π* transitions (nm)*
	*π-π**	*n-π**	
RAInh-1	229	298	-
RAInh-2	229	289	338
RAInh-3	216	281	332
RAInh-4	229	278	323

The ESI-Mass spectra of **RAInh 1-4** show *m/z* peaks corresponding to molecular ion M^+ as well as (M^+-Cl) values (*Table 4.3*). The *m/z* values of the molecular ion peaks for

the complexes indicate that the *p*-cymene and one Schiff base ligand (N, O donor) are coordinated to the metal centre. The mass spectra of all the four complexes have been provided in *Fig. 4.6*.

Table 4.3: *m/z values of complexes* ***RAInh 1-4****showing fragmentation.*

Compound	*m/z values*	*Fragments*
RAInh-1	495.9	$[Ru(\eta^6\text{-}p\text{-cym})(Inh\text{-}1)Cl]^+ +1\ (M^+ +1)$
	460	$[Ru(\eta^6\text{-}p\text{-cym})(Inh\text{-}1)]^+\ (M^+ \text{-} Cl)$
RAInh-2	512.4	$[Ru(\eta^6\text{-}p\text{-cym})(Inh\text{-}2)Cl]^+ +1\ (M^+ +1)$
	475.9	$[Ru(\eta^6\text{-}p\text{-cym})(Inh\text{-}2)]^+\ (M^+ \text{-} Cl)$
RAInh-3	541.3	$[Ru(\eta^6\text{-}p\text{-cym})(Inh\text{-}3)Cl]^+\ (M^+)$
	505.9	$[Ru(\eta^6\text{-}p\text{-cym})(Inh\text{-}3)]^+\ (M^+ \text{-} Cl)$
RAInh-4	526	$[Ru(\eta^6\text{-}p\text{-cym})(Inh\text{-}4)Cl]^+ +1\ (M^+ +1)$
	490	$[Ru(\eta^6\text{-}p\text{-cym})(Inh\text{-}4)]^+\ (M^+ \text{-} Cl)$

The ^{1}H NMR spectra (*Fig. 4.7)* of **RAInh 1-4** show distinct peaks for both *p*-cymene and Schiff base ligands coordinated the Ru(II) centre. The presence of a *p*-cymene ligand on the complexes can be confirmed by the following peaks:
(i) 6 proton doublet at δ= 1.19 ppm owing to two methyl protons of *iso*-propyl group [$CH(CH_3)_2$]; (ii) 3 proton singlet at δ= 2.08 ppm due to the Ar-methyl group *para* to the *iso*-propyl group; (iii) 1 proton quartet at δ= 2.85 ppm attributed to –CH of the *iso*-propyl group; (iv) two 2 proton doublets at δ= 5.8 ppm can be assigned to the 4 Ar-protons of *p*-cymene.

Rest of the peaks are associated with the schiff base ligand. The 1 proton singlet obtained at δ ~12 ppm which was attributed to the N-H proton of the diazenyl group (N=NH) in the ^{1}H NMR spectra of the free ligands (*sec. 2.2.4*) is no more observed in the spectra of their complexes. This is indicative of the enolate structure of the coordinated ligand, which is in line with the IR data and supportive of enolization and deprotonation on coordination to metal via the enolic oxygen. The 1 proton singlet obtained at δ ~12 ppm in the spectra of complexes **RAInh-2** and **RAInh-3** is attributable to the –OH group present in the Schiff base ligand which has shifted downfield on complexation. The peaks in the δ range 7-9 ppm are associated with the aromatic protons as well as the pyridyl-protons of the Schiff base. While the 3 proton singlet peak obtained at δ = 3.8 ppm is due to the $–OCH_3$ group present in the Schiff base ligand of complexes **RAInh-3** and **4**.

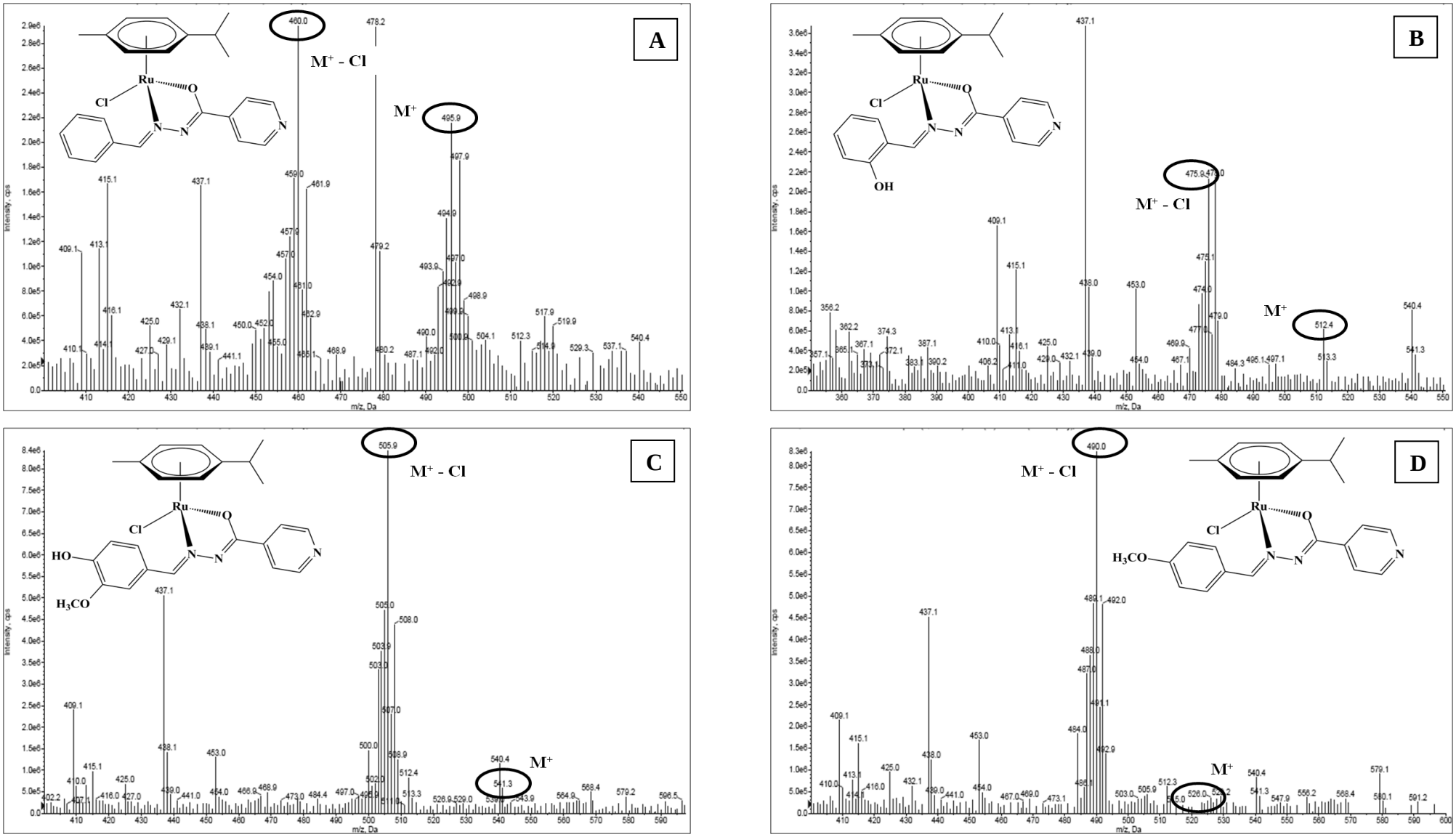

Fig. 4.6: *ESI-MS spectra of complexes (A)* ***RAInh-1*** *(B)* ***RAInh-2*** *(C)* ***RAInh-3*** *(D)* ***RAInh-4*** *indicating their molecular ion peak.*

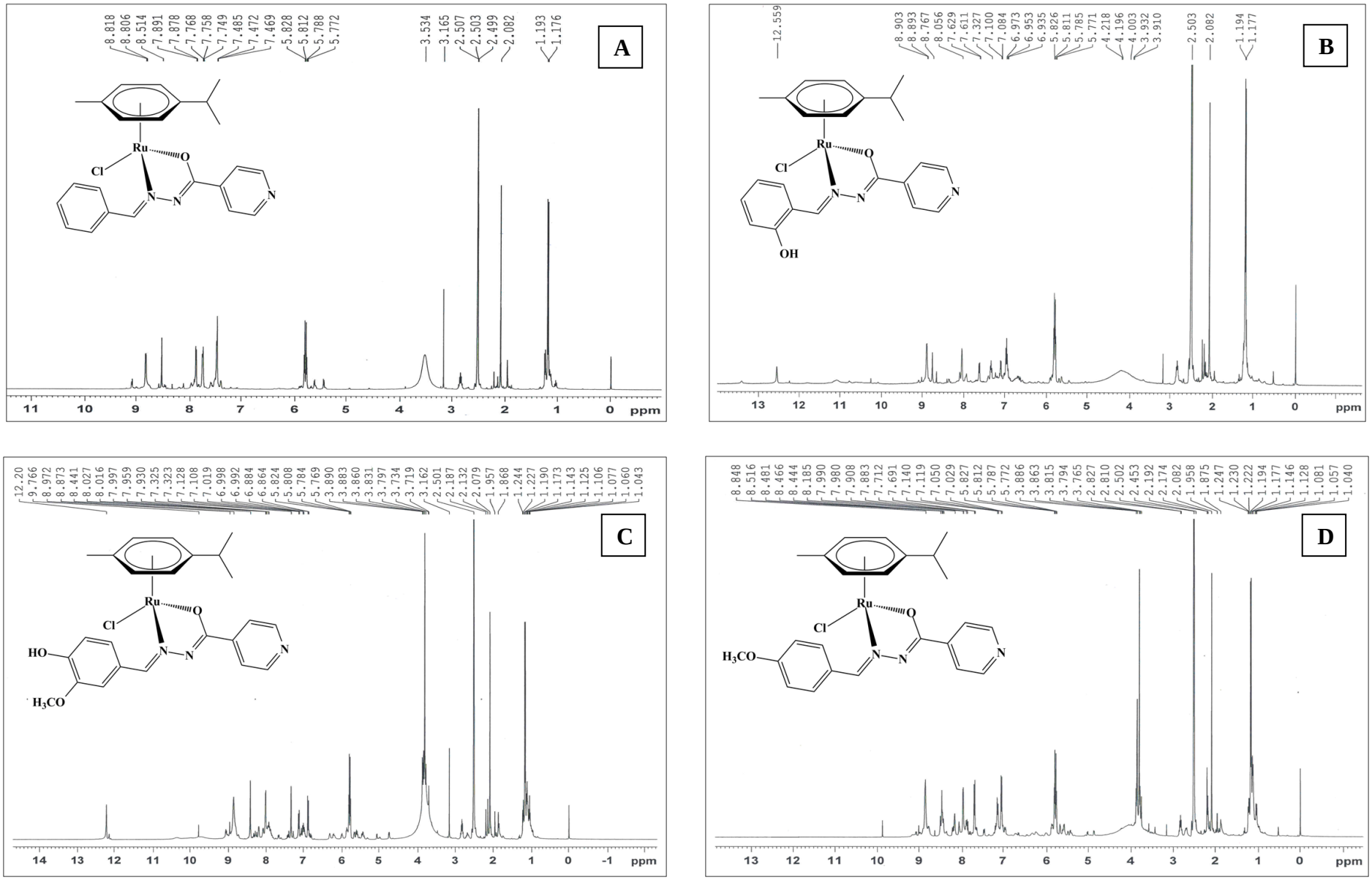

Fig. 4.7: *^{1}H NMR spectra of complexes (A)* ***RAInh-1*** *(B)* ***RAInh-2*** *(C)* ***RAInh-3*** *(D)* ***RAInh-4****.*

4.4 [Ru(η^6-p-cym)(FcA 1-4)Cl] complexes: (RAFcA 1-4)

4.4.1 Synthesis and characterization:

[Ru(η^6-p-cym)(FcA-1)Cl] **(RAFcA-1)**:

RAFcA-1 was synthesized by reaction of [Ru(η^6-*p*-cymene)Cl_2]$_2$ (0.049 mmol, 30.0 mg) and ligand **FcA-1** (0.098 mmol, 37.1 mg). Soluble in almost all organic solvents like DMSO, MeOH, CH_2Cl_2. Yield: 69.1%; Molecular Weight 648.97 g/mole; Molecular Formula $C_{30}H_{35}ClFeNO_3Ru$; Anal. Found: C, 54.01; H, 4.83; N, 2.09. Calc.: C, 55.44; H, 5.43; N, 2.15. ESI-MS *m/z*: 650.1 (M^++1), 614.1 (M^+-Cl); FTIR (KBr/ cm^{-1}): $\nu_{(Ar)C-H}$ 2959, $\nu_{COOassym}$ 1580, ν_{COOsym} 1392, $\Delta\nu_{COO}$ 188.

[Ru(η^6-p-cym)(FcA-2)Cl] **(RAFcA-2)**:

RAFcA-2 was synthesized by reaction of [Ru(η^6-*p*-cymene)Cl_2]$_2$ (0.049 mmol, 30.0 mg) and ligand **FcA-2** (0.098 mmol, 35.6 mg). Soluble in almost all organic solvents like DMSO, MeOH, CH_2Cl_2. Yield: 74.3%; Molecular Weight 633.97 g/mole; Molecular Formula $C_{30}H_{35}ClFeNO_2Ru$; Anal. Found: C, 53.94; H, 4.71; N, 2.00. Calc.: C, 56.84; H, 5.56; N, 2.21. ESI-MS *m/z*: 633.9 (M^+), 597.9 (M^+-Cl); FTIR (KBr/ cm^{-1}): $\nu_{(Ar)C-H}$ 2959, $\nu_{COOassym}$ 1626, ν_{COOsym} 1371, $\Delta\nu_{COO}$ 255.

[Ru(η^6-p-cym)(FcA-3)Cl] **(RAFcA-3)**:

RAFcA-3 was synthesized by reaction of [Ru(η^6-*p*-cymene)Cl_2]$_2$ (0.049 mmol, 30.0 mg) and ligand **FcA-3** (0.098 mmol, 32.3 mg). Soluble in almost all organic solvents like DMSO, MeOH, CH_2Cl_2. Yield: 77.9%; Molecular Weight 599.96 g/mole; Molecular Formula $C_{27}H_{37}ClFeNO_2Ru$; Anal. Found: C, 51.72; H, 5.91; N, 2.14. Calc.: C, 54.05; H, 6.22; N, 2.33. ESI-MS *m/z*: 599.9 (M^+), 563.9 (M^+-Cl); FTIR (KBr/ cm^{-1}): $\nu_{(Ar)C-H}$ 2957, $\nu_{COOassym}$ 1627, ν_{COOsym} 1374, $\Delta\nu_{COO}$ 253.

[Ru(η^6-p-cym)(FcA-4)Cl] **(RAFcA-4)**:

RAFcA-4 was synthesized by reaction of [Ru(η^6-*p*-cymene)Cl_2]$_2$ (0.049 mmol, 30.0 mg) and ligand **FcA-4** (0.098 mmol, 39.4 mg). Soluble in almost all organic solvents like DMSO, MeOH, CH_2Cl_2. Yield: 69.9%; Molecular Weight 673.01 g/mole; Molecular Formula $C_{32}H_{36}ClFeN_2O_2Ru$; Anal. Found: C, 53.51; H, 5.52; N, 3.83. Calc.: C, 57.11; H, 5.39; N, 4.16. ESI-MS *m/z*: 672.9 (M^+), 636.9 (M^+-Cl); FTIR (KBr/ cm^{-1}): $\nu_{(Ar)C-H}$ 2962, $\nu_{COOassym}$ 1622, ν_{COOsym} 1386, $\Delta\nu_{COO}$ 236.

4.4.2 Results and discussion:

The IR spectra of the complexes **RAFcA 1-4** displayed characteristic strong stretching bands at 1580-1630 cm^{-1} and weaker bands at 1370-1395 cm^{-1} due to asymmetric and symmetric carboxylate (COO^-) stretch respectively which were found as strong bands in the fingerprint region at 1580-1610 cm^{-1} in the spectra of free ligands **FcA 1-4** (*Sec. 2.3.4*). The separation frequency Δν values fall in the range 188–255 cm^{-1} indicating a monodentate coordination mode of the carboxylato group of the ligand to the metal [25,26]. The distinct broad band at ~3450 cm^{-1} owing to the O-H stretching of free carboxylic acid group found in the ligand is completely lost in the IR spectra of the complex indicating complexation of the ligand with metal via the carboxylate oxygen. Furthermore the medium secondary amine N-H stretching bands found in the spectra of the free ligands in the region of 2900-3000 cm^{-1} was found to have a positive shift in the region of 3050-3200 cm^{-1} in complexes indicating complexation of the ligand with metal via the nitrogen of secondary amine (mannich base). The presence of weak to medium bands in the fingerprint regions 2900-3000 cm^{-1} owing to aromatic ν_{C-H} stretch and strong bands around 1430-1667 cm^{-1} due to the aromatic $\nu_{C=C}$ in plane vibrations is indicative of presence of *p*-cymene in the complex.

The electronic absorption spectra of the complexes **RAFcA 1-4** recorded in DMSO solution showed absorption bands in the region 200-500 nm. The electronic spectra of free ligands **FcA 1-4** displayed intense absorption bands at 207-209 nm ascribable to intra ligand $\pi \rightarrow \pi^*$ transition of the cyclopentadienyl rings of ferrocene (*Fig. 2.8, Sec. 2.3.4*) which were observed to have shifted to longer wavelength region at 260-280 nm (*Fig. 4.8*) due to coordination with Ru(II) metal centre. All the four complexes showed broad shoulder peaks in the region 300-340 nm corresponding to $n \rightarrow \pi^*$ transitions, whereas the MLCT transitions have been obtained as broad peaks in the region 370-420 nm. The absorption peak values have been tabulated in *Table 4.4*.

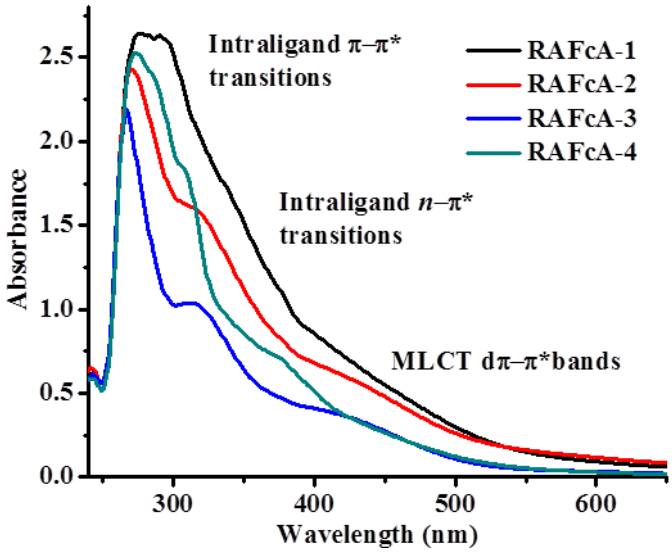

Fig. 4.8: *UV-vis. spectra of complexes* ***RAFcA 1-4*** *recorded in DMSO with path length 1 cm.*

Table 4.4: *UV-Vis. peak assignments of* ***RAFcA 1-4***

Compound	***Intra-ligand transitions (nm)***		***MLCT dπ-π* transitions (nm)***
	π-π*	***n-π****	
RAFcA-1	277	336	-
RAFcA-2	271	318	407
RAFcA-3	266	316	420
RAFcA-4	274	308	373

The ESI-Mass spectra of **RAFcA 1-4** show *m/z* peaks corresponding to molecular ion M^+ as well as (M^+-Cl) values (*Table 4.5*). The mass spectra of all the four complexes have been provided in *Fig. 4.9*.

Table 4.5: *m/z values of complexes* ***RAFcA 1-4****showing fragmentation.*

Compound	***m/z values***	***Fragments***
RAFcA-1	650.1	$[Ru(\eta^6\text{-}p\text{-cym})(FcA\text{-}1)Cl]^+$ +1 (M^++1)
	614.1	$[Ru(\eta^6\text{-}p\text{-cym})(FcA\text{-}1)]^+$ (M^+-Cl)
RAFcA-2	633.9	$[Ru(\eta^6\text{-}p\text{-cym})(FcA\text{-}2)Cl]^+$ (M^+)
	597.9	$[Ru(\eta^6\text{-}p\text{-cym})(FcA\text{-}2)]^+$ (M^+-Cl)
RAFcA-3	599.9	$[Ru(\eta^6\text{-}p\text{-cym})(FcA\text{-}3)Cl]^+$ (M^+)
	563.9	$[Ru(\eta^6\text{-}p\text{-cym})(FcA\text{-}3)]^+$ (M^+-Cl)
RAFcA-4	672.9	$[Ru(\eta^6\text{-}p\text{-cym})(FcA\text{-}4)Cl]^+$ (M^+)
	636.9	$[Ru(\eta^6\text{-}p\text{-cym})(FcA\text{-}4)]^+$ (M^+-Cl)

Due to poor solubilities of **RAFcA 1-4**, their ^{1}H NMR spectra with good resolution could not be obtained hence not discussed.

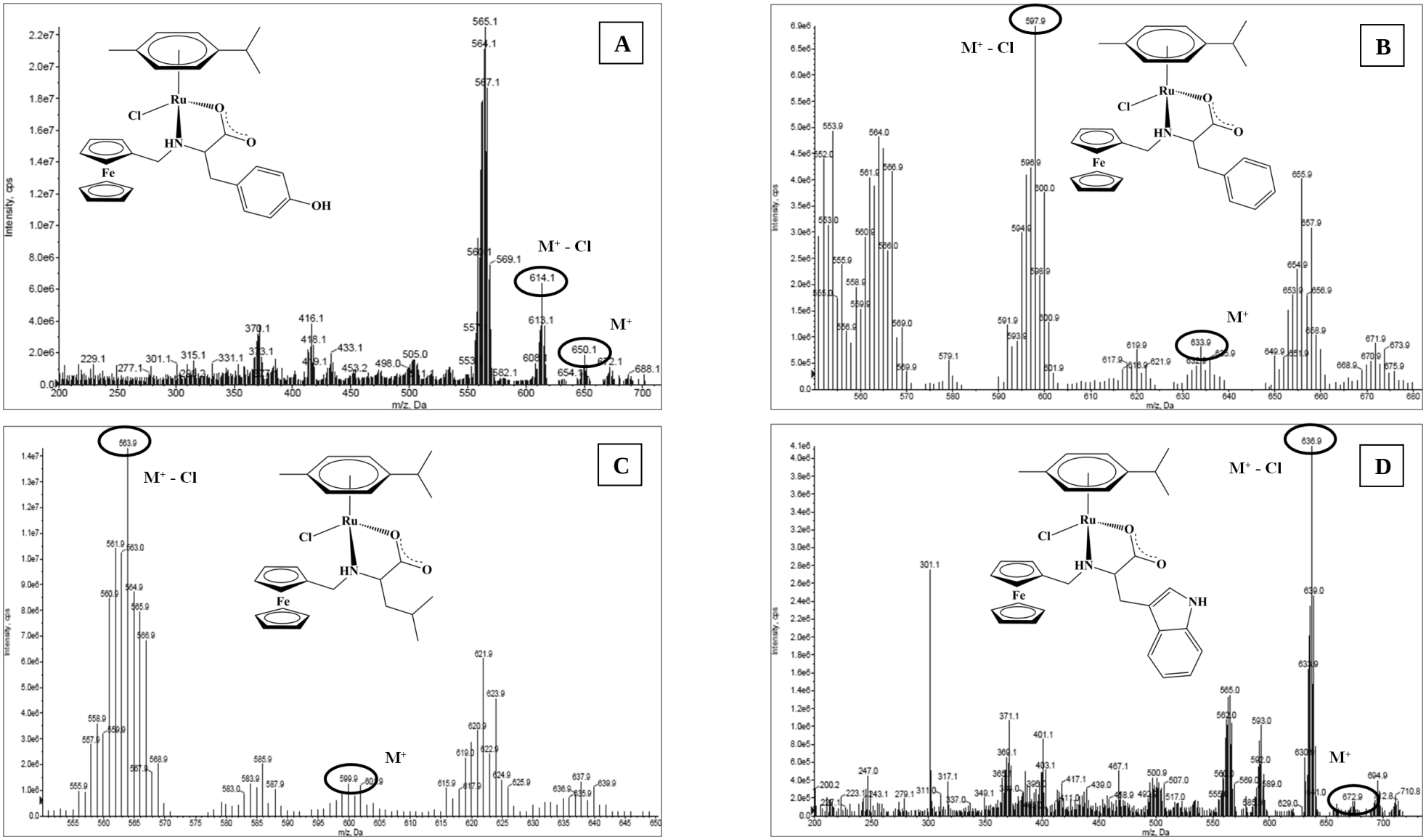

Fig. 4.9: *ESI-MS spectra of complexes (A)* ***RAFcA-1*** *(B)* ***RAFcA-2*** *(C)* ***RAFcA-3*** *(D)* ***RAFcA-4*** *indicating their molecular ion peak.*

4.5 [Ru(η^6-p-cym)(Stb 1-4)Cl_2] complexes: (RAStb 1-4)

4.5.1 Synthesis and characterization:

[Ru(η^6-p-cym)(Stb-1)Cl_2] **(RAStb-1)**:

RAStb-1 was synthesized by reaction of [Ru(η^6-*p*-cymene)Cl_2]$_2$ (0.049 mmol, 30.0 mg) and ligand **Stb-1** (0.098 mmol, 17.7 mg). Soluble in almost all organic solvents like DMSO, MeOH, CH_2Cl_2. Yield: 78.5%; Molecular Weight 487.43 g/mole; Molecular Formula $C_{23}H_{25}Cl_2NRu$; Anal. Found: C, 51.97; H, 4.69; N, 2.28. Calc.: C, 56.67; H, 5.17; N, 2.87. ESI-MS *m/z*: 489.1 (M^++1), 453.0 (M^+-Cl); δ_H (400 MHz, DMSO-d_6): 8.80 (d, 2H, pyridyl α-H), 7.68-7.63 (dd, 2H, pyridyl β-H), 7.45-7.38 (m, 5H, Ar-H), 7.36 (d, J_{trans} 14.0, 1H, HC=CH), 7.31 (d, J_{trans} 16.4, 1H, HC=CH), 5.82-5.77 (m, 4H, *p*-cym Ar-H), 2.84-2.81 (q, 1H, *p*-cym-*iso*-prop-CH), 2.08 (s, 3H, *p*-cym Ar-CH_3), 1.19 (d, 6H, *p*-cym-*iso*-prop-$(CH_3)_2$); FTIR (KBr/ cm^{-1}): $\nu_{(Ar)C-H}$ 2959, $\nu_{C=N(py)}$ 1498(s).

[Ru(η^6-p-cym)(Stb-2)Cl_2] **(RAStb-2)**:

RAStb-2 was synthesized by reaction of [Ru(η^6-*p*-cymene)Cl_2]$_2$ (0.049 mmol, 30.0 mg) and ligand **Stb-2** (0.098 mmol, 20.7 mg). Soluble in almost all organic solvents like DMSO, MeOH, CH_2Cl_2. Yield: 66.9%; Molecular Weight 517.45 g/mole; Molecular Formula $C_{24}H_{27}Cl_2NORu$; Anal. Found: C, 52.59; H, 5.11; N, 2.91. Calc.: C, 55.71; H, 5.26; N, 2.71. ESI-MS *m/z*: 516.0 (M^+-1), 482.0 (M^+-Cl); δ_H (400 MHz, DMSO-d_6): 8.76 (d, 2H, pyridyl α-H), 7.62-7.49 (dd, 2H, pyridyl β-H), 7.19 (d, J_{trans} 14.0, 1H, HC=CH), 7.12 (d, J_{trans} 16.4, 1H, HC=CH), 7.01-6.97 (m, 4H, Ar-H), 5.82-5.77 (m, 4H, *p*-cym Ar-H), 3.79 (s, 3H, OCH_3), 2.84-2.79 (q, 1H, *p*-cym-*iso*-prop-CH), 2.08 (s, 3H, *p*-cym Ar-CH_3), 1.19 (d, 6H, *p*-cym-*iso*-prop-$(CH_3)_2$); FTIR (KBr/ cm^{-1}): $\nu_{(Ar)C-H}$ 2964, $\nu_{C=N(py)}$ 1510(s), $\nu_{ArC=C}$ 1597(s).

[Ru(η^6-p-cym)(Stb-3)Cl_2] **(RAStb-3)**:

RAStb-3 was synthesized by reaction of [Ru(η^6-*p*-cymene)Cl_2]$_2$ (0.049 mmol, 30.0 mg) and ligand **Stb-3** (0.098 mmol, 22.2 mg). Soluble in almost all organic solvents like DMSO, MeOH, CH_2Cl_2. Yield: 74.3%; Molecular Weight 532.42 g/mole; Molecular Formula $C_{23}H_{24}Cl_2N_2O_3Ru$; Anal. Found: C, 48.86; H, 3.92; N, 5.04. Calc.: C, 51.88; H, 4.54; N, 5.26. ESI-MS *m/z*: 497.2 (M^+-Cl); δ_H (400 MHz, DMSO-d_6): 8.86 (d, 2H, pyridyl α-H), 8.30-8.26 (dd, 2H, pyridyl β-H), 7.96-7.92 (dd, 2H, Ar-H), 7.75 (d, J_{trans} 16.4, 1H, HC=CH), 7.70 (d, 2H, Ar-H), 7.56 (d, J_{trans} 16.4, 1H, HC=CH), 5.82-5.77 (m, 4H, *p*-cym Ar-H), 2.84-2.81 (q, 1H, *p*-cym-*iso*-prop-CH), 2.08 (s, 3H, *p*-cym Ar-CH_3),

1.19 (d, 6H, *p*-cym-*iso*-prop-$(CH_3)_2$); FTIR (KBr/ cm^{-1}): $\nu_{(Ar)C-H}$ 2961, $\nu_{C=N(py)}$ 1510(s), $\nu_{ArC=C}$ 1603(s).

[Ru(η^6-p-cym)(Stb-4)Cl_2] **(RAStb-4)**:

RAStb-4 was synthesized by reaction of $[Ru(\eta^6\text{-}p\text{-cymene})Cl_2]_2$ (0.049 mmol, 30.0 mg) and ligand **Stb-4** (0.098 mmol, 19.5 mg). Soluble in almost all organic solvents like DMSO, MeOH, CH_2Cl_2. Yield: 71.1%; Molecular Weight 505.42 g/mole; Molecular Formula $C_{23}H_{24}Cl_2FNRu$; Anal. Found: C, 51.79; H, 4.38; N, 2.85. Calc.: C, 54.66; H, 4.79; N, 2.77. ESI-MS *m/z*: 470.3 (M^+-Cl); δ_H (400 MHz, DMSO-d_6): 8.80 (d, 2H, pyridyl α-H), 8.69-8.26 (d, 2H, pyridyl β-H), 7.76-7.56 (m, 4H, Ar-H), 7.30 (d, J_{trans} 17.0, 1H, HC=CH), 7.25 (d, J_{trans} 16.8, 1H, HC=CH), 5.82-5.77 (m, 4H, *p*-cym Ar-H), 2.84-2.79 (q, 1H, *p*-cym-*iso*-prop-CH), 2.08 (s, 3H, *p*-cym Ar-CH_3), 1.19 (d, 6H, *p*-cym-*iso*-prop-$(CH_3)_2$); FTIR (KBr/ cm^{-1}): $\nu_{(Ar)C-H}$ 2965, $\nu_{C=N(py)}$ 1510(s), $\nu_{ArC=C}$ 1598(s).

4.5.2 Results and discussion:

Strong band at around 1500-1508 cm^{-1} owing to the C=N stretching of the pyridine ring in the ligands **Stb 1-4** (*sec. 2.4.4*) were found to have shifted to slightly higher wavenumber at 1510 cm^{-1} in **RAStb 1-4** indicating coordination of the pyridyl N to the metal centre. Moreover the presence of weak to medium bands in the fingerprint regions 2900-3000 cm^{-1} owing to aromatic ν_{C-H} stretch and strong bands around 1430-1667 cm^{-1} due to the aromatic $\nu_{C=C}$ in plane vibrations is indicative of presence of *p*-cymene in the complex.

The electronic absorption spectra of the complexes **RAStb 1-4** recorded in DMSO solution were found to show bands in the region 200-500 nm. The electronic spectra of free ligands **Stb 1-4** displayed intense absorption band at ~ 223 nm due to the intra-ligand $\pi\rightarrow\pi^*$ transitions which remains unchanged whereas the $n\rightarrow\pi^*$ transition (*Fig. 2.12, Sec. 2.4.4*) seems to have shifted to slightly smaller wavelength in case of **RAStb-1** while the same is observed to have remained unchanged in case of **RAStb-2** to **4** (*Fig. 4.10*). A MLCT band at 394 nm was observed for complex **RAStb-1**. The absorption peak values have been tabulated in *Table 4.6*.

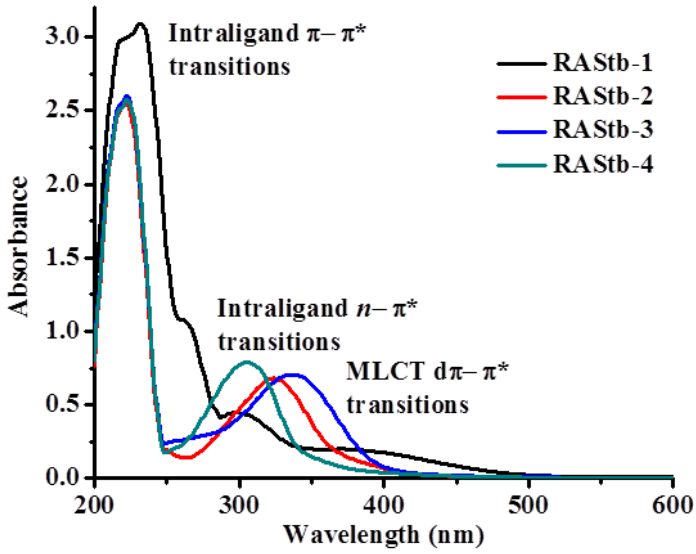

Fig. 4.10: *UV-vis. spectra of complexes* ***RAStb 1-4*** *recorded in DMSO with path length 1 cm.*

Table 4.6: *UV-Vis. peak assignments of* ***RAStb 1-4***

Compound	*Intra-ligand transitions (nm)*	
	π-π*	***n-π****
RAStb-1	230	301
RAStb-2	222	324
RAStb-3	221	339
RAStb-4	223	307

The ESI-Mass spectra of **RAStb 1-4** show *m/z* peaks corresponding to molecular ion M^+ as well as (M^+-Cl) values (*Table 4.7*). The mass spectra of all the four complexes have been provided in *Fig. 4.11*.

Table 4.7: *m/z values of complexes* ***RAStb 1-4****showing fragmentation.*

Compound	*m/z values*	*Fragments*
RAStb-1	489.1	$[Ru(\eta^6\text{-}p\text{-cym})(Stb\text{-}1)Cl]^+$ +1 (M^++1)
	453	$[Ru(\eta^6\text{-}p\text{-cym})(Stb\text{-}1)]^+$ (M^+-Cl)
RAStb-2	516	$[Ru(\eta^6\text{-}p\text{-cym})(Stb\text{-}2)Cl]^+$ -1 (M^+-1)
	482	$[Ru(\eta^6\text{-}p\text{-cym})(Stb\text{-}2)]^+$ (M^+-Cl)
RAStb-3	497.2	$[Ru(\eta^6\text{-}p\text{-cym})(Stb\text{-}3)]^+$ (M^+-Cl)
RAStb-4	470.3	$[Ru(\eta^6\text{-}p\text{-cym})(Stb\text{-}4)]^+$ (M^+-Cl)

The ^{1}H NMR spectra (*Fig. 4.12)* of **RAStb 1-4** show peaks for *p*-cymene at the same δ values as is discussed in *sec. 4.3.2*. Apart from those; peaks owing to the stilbene ligands are also in well accordance with the peaks of the free ligands (*Sec. 2.4.4*). All the four complexes show pyridyl peaks for α and β protons at ~ 8.8 ppm and ~ 7.6-8.6 ppm respectively. The two, single proton doublets in the region 7.1-7.7 ppm with J = 16.4 confirms the presence of *trans* alkene (HC=CH). While the 3 proton singlet peak obtained at δ=3.79 ppm is due to the $–OCH_3$ group present in the stilbene derivative of complexe **RAStb-2**.

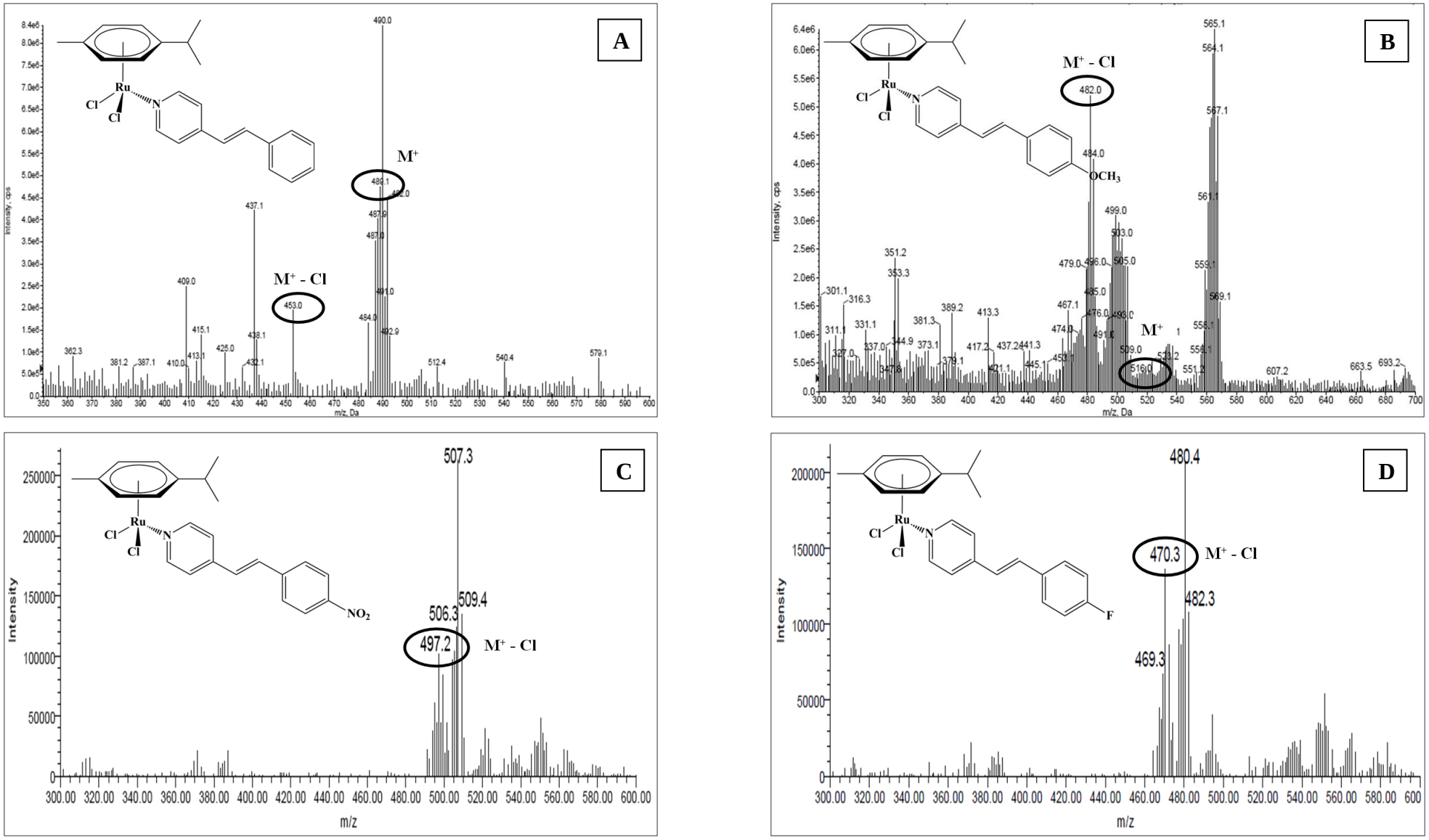

Fig. 4.11: *ESI-MS spectra of complexes (A)* ***RAStb-1*** *(B)* ***RAStb-2*** *(C)* ***RAStb-3*** *(D)* ***RAStb-4*** *indicating their molecular ion peak.*

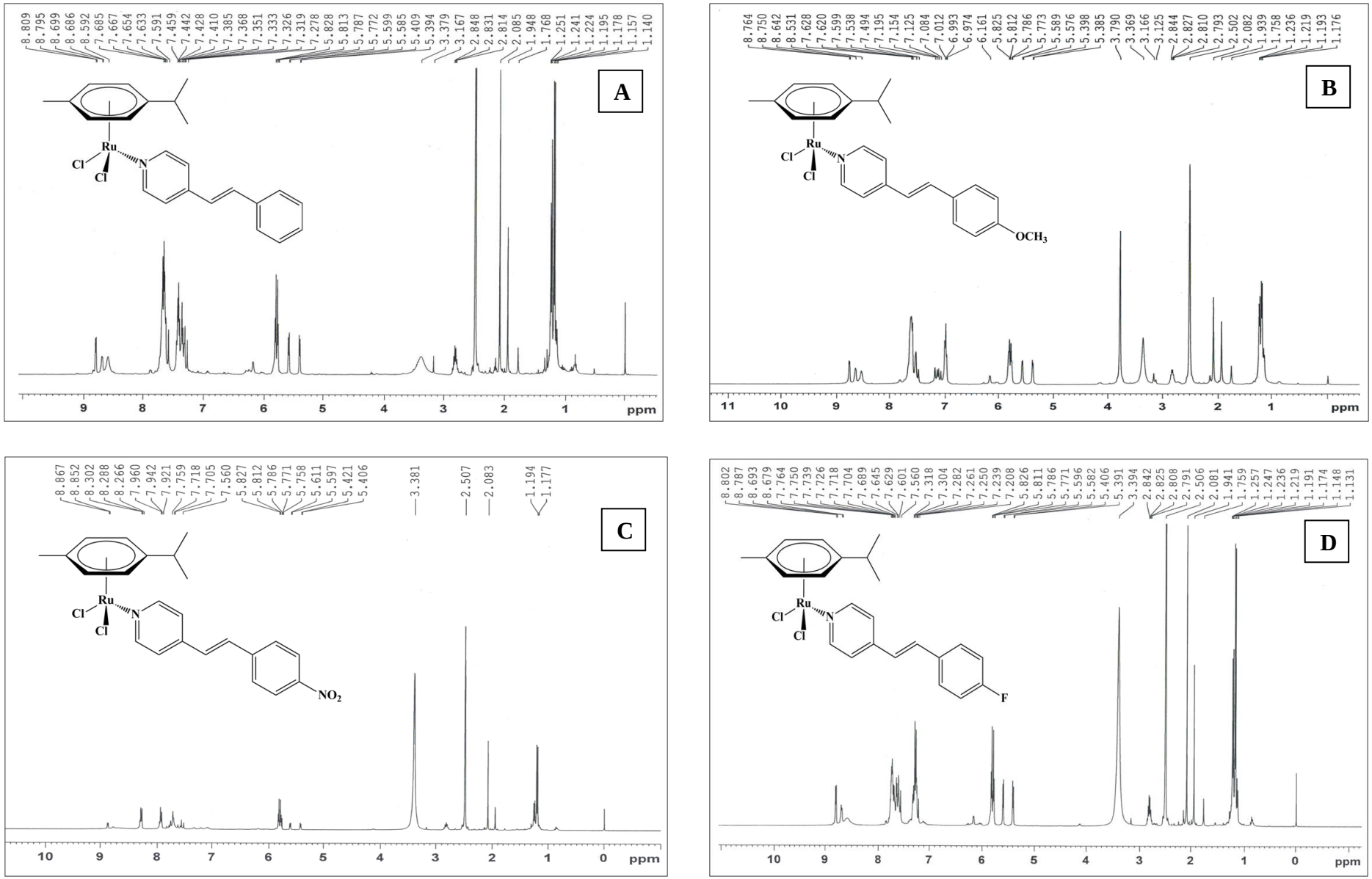

Fig. 4.12: *^{1}H NMR spectra of complexes (A)* ***RAStb-1*** *(B)* ***RAStb-2*** *(C)* ***RAStb-3*** *(D)* ***RAStb-4****.*

4.6 [Ru(η^6-p-cym)(Isa 1-4)Cl] complexes: (RAIsa 1-4)

4.6.1 Synthesis and characterization:

[Ru(η^6-p-cym)(Isa-1)Cl] **(RAIsa-1)**:

RAIsa-1 was synthesized by reaction of $[Ru(\eta^6\text{-}p\text{-cymene})Cl_2]_2$ (0.049 mmol, 30.0 mg) and ligand **Isa-1** (0.098 mmol, 25.9 mg). Soluble in almost all organic solvents like DMSO, MeOH, CH_2Cl_2. Yield: 62.8%; Molecular Weight 535.00 g/mole; Molecular Formula $C_{25}H_{24}ClN_3O_2Ru$; Anal. Found: C, 52.49; H, 4.51; N, 6.97. Calc.: C, 56.12; H, 4.52; N, 7.85. ESI-MS *m/z*: 535.1 (M^+), 500.1 (M^+-Cl); δ_H (400 MHz, DMSO-d_6) 11.39 (s, 1H, indolinic NH), 7.91-7.89 (dd, 1H, indolinic Ar-H), 7.69-7.60 (m, 5H, Ar-H), 7.42-7.38 (dt, 1H, indolinic Ar-H), 7.14-7.10 (t, 1H, indolinic Ar-H), 6.97-6.95 (d, 1H, indolinic Ar-H), 5.86-5.77 (m, 4H, *p*-cym Ar-H), 2.84-2.81 (q, 1H, *p*-cym-*iso*-prop-CH), 2.08 (s, 3H, *p*-cym Ar-CH_3), 1.19 (d, 6H, *p*-cym-*iso*-prop-$(CH_3)_2$); FTIR (KBr/ cm^{-1}): $\nu_{(indolinic)N\text{-}H}$ 3235, $\nu_{(Ar)C\text{-}H}$ 2960, $\nu_{(indolinic)C=O}$ 1693, $\nu_{C=N}$ 1535, $\nu_{C\text{-}O}$ 1094.

[Ru(η^6-p-cym)(Isa-2)Cl] **(RAIsa-2)**:

RAIsa-2 was synthesized by reaction of $[Ru(\eta^6\text{-}p\text{-cymene})Cl_2]_2$ (0.049 mmol, 30.0 mg) and ligand **Isa-2** (0.098 mmol, 26.1 mg). Soluble in almost all organic solvents like DMSO, MeOH, CH_2Cl_2. Yield: 65.1%; Molecular Weight 535.99 g/mole; Molecular Formula $C_{24}H_{23}ClN_4O_2Ru$; Anal. Found: C, 50.15; H, 3.86; N, 9.55. Calc.: C, 53.78; H, 4.33; N, 10.45. ESI-MS *m/z*: 534.9 (M^+), 500.9 (M^+-Cl); δ_H (400 MHz, DMSO-d_6) 11.45 (s, 1H, indolinic NH), 8.88 (d, 2H, pyridinyl α-H), 7.80-7.79 (d, 2H, pyridinyl β-H), 7.61 (broad s, 1H, indolinic Ar-H), 7.43-7.39 (t, 1H, indolinic Ar-H), 7.13-7.10 (t, 1H, indolinic Ar-H), 6.98-6.96 (d, 1H, indolinic Ar-H), 5.82-5.76 (m, 4H, *p*-cym Ar-H), 2.84-2.79 (q, 1H, *p*-cym-*iso*-prop-CH), 2.08 (s, 3H, *p*-cym Ar-CH_3), 1.19 (d, 6H, *p*-cym-*iso*-prop-$(CH_3)_2$); FTIR (KBr/ cm^{-1}): $\nu_{(indolinic)N\text{-}H}$ 3205, $\nu_{(Ar)C\text{-}H}$ 2959, $\nu_{(indolinic)C=O}$ 1700, $\nu_{C=N}$ 1538, $\nu_{C\text{-}O}$ 1093.

[Ru(η^6-p-cym)(Isa-3)Cl] **(RAIsa-3)**:

RAIsa-3 was synthesized by reaction of $[Ru(\eta^6\text{-}p\text{-cymene})Cl_2]_2$ (0.049 mmol, 30.0 mg) and ligand **Isa-3** (0.098 mmol, 20.0 mg). Soluble in almost all organic solvents like DMSO, MeOH, CH_2Cl_2. Yield: 71.5%; Molecular Weight 473.92 g/mole; Molecular Formula $C_{19}H_{21}ClN_4O_2Ru$; Anal. Found: C, 45.76; H, 4.35; N, 10.73. Calc.: C, 48.15; H, 4.47; N, 11.82. ESI-MS *m/z*: 473.9 (M^+), 439.0 (M^+-Cl); δ_H (400 MHz, DMSO-d_6) 10.74 (s, 1H, indolinic NH), 10.21 (s, 2H, NH_2), 8.1-8.08 (d, 1H, indolinic Ar-H), 7.33-7.31 (dt, 1H, indolinic Ar-H), 7.04-7.02 (t, 1H, indolinic Ar-H), 6.91–6.89 (d, 1H, indolinic Ar-H),

5.82-5.77 (m, 4H, *p*-cym Ar-H), 2.85-2.78 (q, 1H, *p*-cym-*iso*-prop-CH), 2.08 (s, 3H, *p*-cym Ar-CH_3), 1.19 (d, 6H, *p*-cym-*iso*-prop-$(CH_3)_2$); FTIR (KBr/ cm^{-1}): $\nu_{(indolinic)N-H}$ 3157, $\nu_{(Ar)C-H}$ 2962, $\nu_{(indolinic)C=O}$ 1726, $\nu_{C=N}$ 1555, ν_{C-O} 1110.

[Ru(η^6-p-cym)(Isa-4)Cl] **(RAIsa-4)**:

RAIsa-4 was synthesized by reaction of $[Ru(\eta^6\text{-}p\text{-cymene})Cl_2]_2$ (0.049 mmol, 30.0 mg) and ligand **Isa-4** (0.098 mmol, 21.5 mg). Soluble in almost all organic solvents like DMSO, MeOH, CH_2Cl_2. Yield: 69.3%; Molecular Weight 489.98 g/mole; Molecular Formula $C_{19}H_{21}ClN_4ORuS$; Anal. Found: C, 43.94; H, 4.59; N, 10.12. Calc.: C, 46.57; H, 4.32; N, 11.43. ESI-MS *m/z*: 485.1 (M^+-4), 453.0 (M^+-Cl-2); δ_H (400 MHz, DMSO-d_6) 11.21 (s, 1H, indolinic NH), 10.58 (s, 2H, NH_2), 9.47-9.45 (d, *J* 7.2, 1H, indolinic Ar-H), 7.47-7.38 (t, 1H, indolinic Ar-H), 7.13-7.10 (t, 1H, indolinic Ar-H), 7.08–7.06 (d, 1H, indolinic Ar-H), 5.81-5.34 (m, 4H, *p*-cym Ar-H), 2.83-2.77 (q, 1H, *p*-cym-*iso*-prop-CH), 2.08 (s, 3H, *p*-cym Ar-CH_3), 1.20 (d, 6H, *p*-cym-*iso*-prop-$(CH_3)_2$); FTIR (KBr/ cm^{-1}): $\nu_{(indolinic)N-H}$ 3265, $\nu_{(Ar)C-H}$ 2924, $\nu_{(indolinic)C=O}$ 1698, $\nu_{C=N}$ 1557, ν_{C-S} 876.

4.6.2 Results and discussion:

The IR spectra of complexes **RAIsa 1-4** lack the strong secondary amide carbonyl absorption at 1680–1700 cm^{-1} that is typically seen in the spectra of the free ligands **Isa 1-4** (*sec. 2.5.4*). In all the complexes, $\nu_{C=N}$ band is shifted to lower frequency between 1530-1560 cm^{-1} indicating coordination of the Schiff bases through the azomethine nitrogen. The enolate structure of the coordinated ligand is supported by bands in the range of 1050-1170 cm^{-1} due to the enolic C-O stretching (C-S stretching at 876 cm^{-1} in case of **RAIsa-4**). The broad band found in the range of 3550-3600 cm^{-1} in the IR spectra of free ligands **Isa 1-4** due to the free amide N-H stretch are lost in the IR spectra of their complexes **RAIsa 1-4** which is also indicative of the enolization and deprotonation on coordination to the metal centre. The N-H stretching bands found in the range of 3150-3250 cm^{-1} are attributable to the indolinic N-H. Moreover the presence of weak to medium bands in the fingerprint regions 2900-3000 cm^{-1} owing to aromatic ν_{C-H} stretch and strong bands around 1430-1667 cm^{-1} due to the aromatic $\nu_{C=C}$ in plane vibrations is indicative of presence of *p*-cymene in the complex.

The electronic absorption spectra of the **RAIsa 1-4** complexes (*Fig. 4.13*) show three major bands in the wavelength range 200-400 nm also observed in the free ligands **Isa 1-4**. The first band appearing at ~ 226 nm is attributable to the intraligand $\pi \rightarrow \pi^*$ transition of the aromatic rings of the arene ligand (*p*-cymene) as well as the isatin hydrazone (Isa). The second and third bands observed within 260-350 nm region are due to the intra-

ligand N, O centred $n \rightarrow \pi^*$ transitions which are observed to have shifted to slightly higher wavelength than those found in the free ligand **Isa 1-4** (*Fig. 2.17, Sec. 2.5.4*). This shift in the wavelength indicates coordination of the hydrazone ligand to the metal centre via N, O atoms. MLCT transitions of the complexes are obtained in a range of 390-410 nm as broad peaks with an exception of the complex **RAIsa-4** whose MLCT is seen at a longer wavelength (604 nm). The λ_{max} values of all the transitions taking place in **RAIsa 1-4** have been tabulated in *Table 4.8*.

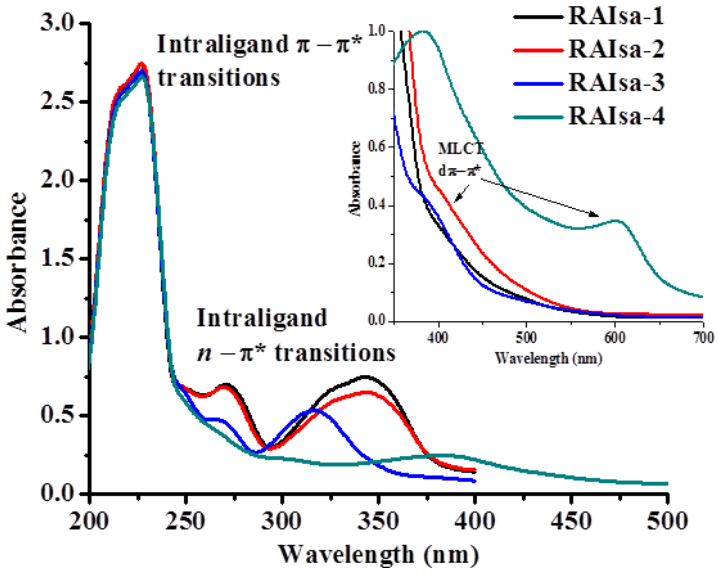

Fig. 4.13: *UV-vis. spectra of complexes* ***RAIsa 1-4*** *recorded in DMSO with path length 1 cm. (Inset: MLCT bands of* ***RAIsa 1-4*** *observed at higher concentrations)*

Table 4.8: *UV-Vis. peak assignments of* ***RAIsa 1-4***

Compound	***Intra-ligand transitions (nm)***		***MLCT dπ-π* transitions (nm)***
	π-π*	***n-π****	
RAIsa-1	226	273, 341	406
RAIsa-2	227	270, 343	410
RAIsa-3	226	269, 316	391
RAIsa-4	226	265, 304	604

The ESI-Mass spectra of **RAIsa 1-4** show *m/z* peaks corresponding to molecular ion M^+ as well as (M^+-Cl) values (*Table 4.9*). In case of complexes **2-4**, peak corresponding to the fragment [Ru(η^6-*p*-xylene)(3-hydrazinylindolin-2-one)]$^+$ at *m/z* = 371 is observed as one of the prominent peak. The *m/z* values of the molecular ion peaks for the complexes indicate that the *p*-cymene and one Schiff base ligand are coordinated to the metal centre. The mass spectra of all the four complexes have been provided in *Fig. 4.14*.

Table 4.9: *m/z values of complexes* ***RAIsa 1-4****showing fragmentation.*

Compound	*m/z values*	*Fragments*
RAIsa-1	535.1	$[Ru(\eta^6\text{-}p\text{-cym})(Isa\text{-}1)Cl]^+$ (M^+)
	500.1	$[Ru(\eta^6\text{-}p\text{-cym})(Isa\text{-}1)]^+$ $(M^+\text{-}Cl)$
RAIsa-2	534.9	$[Ru(\eta^6\text{-}p\text{-cym})(Isa\text{-}2)Cl]^+$ (M^+)
	500.9	$[Ru(\eta^6\text{-}p\text{-cym})(Isa\text{-}2)]^+$ $(M^+\text{-}Cl)$
	371.1	$[Ru(\eta^6\text{-}p\text{-xylene})(3\text{-hydrazinylindolin-2-one})]^+$
RAIsa-3	473.9	$[Ru(\eta^6\text{-}p\text{-cym})(Isa\text{-}3)Cl]^+$ (M^+)
	439	$[Ru(\eta^6\text{-}p\text{-cym})(Isa\text{-}3)]^+$ $(M^+\text{-}Cl)$
	371.0	$[Ru(\eta^6\text{-}p\text{-xylene})(3\text{-hydrazinylindolin-2-one})]^+$
RAIsa-4	485.1	$[Ru(\eta^6\text{-}p\text{-cym})(Isa\text{-}4)Cl]^+$ - 4 $(M^+\text{-}4)$
	453.0	$[Ru(\eta^6\text{-}p\text{-cym})(Isa\text{-}4)]^+$ $(M^+\text{-}Cl\text{-}2)$
	371.1	$[Ru(\eta^6\text{-}p\text{-xylene})(3\text{-hydrazinylindolin-2-one})]^+$

The ^{1}H NMR spectra of the complexes **RAIsa 1-4** (*Fig. 4.15*) are in well agreement with their proposed structures. The peaks corresponding to *p*-cymene appeared at the same δ values as is discussed in *sec. 4.3.2*. The indolinic N-H shows a one proton singlet at a δ value of ~11.4-10.7 ppm whereas the N-H proton of the diazenyl group (N=NH) which appeared as a one proton singlet at a δ value of ~14-12.5 ppm in the free ligands (*Sec. 2.5.4*) is lost in the spectra of their complexes confirming coordination of the ligand through the diazenyl nitrogen of isatin schiff bases. Rest of the signals can be attributed to the aromatic protons of the indolinic ring and the substitution on the diazenyl group.

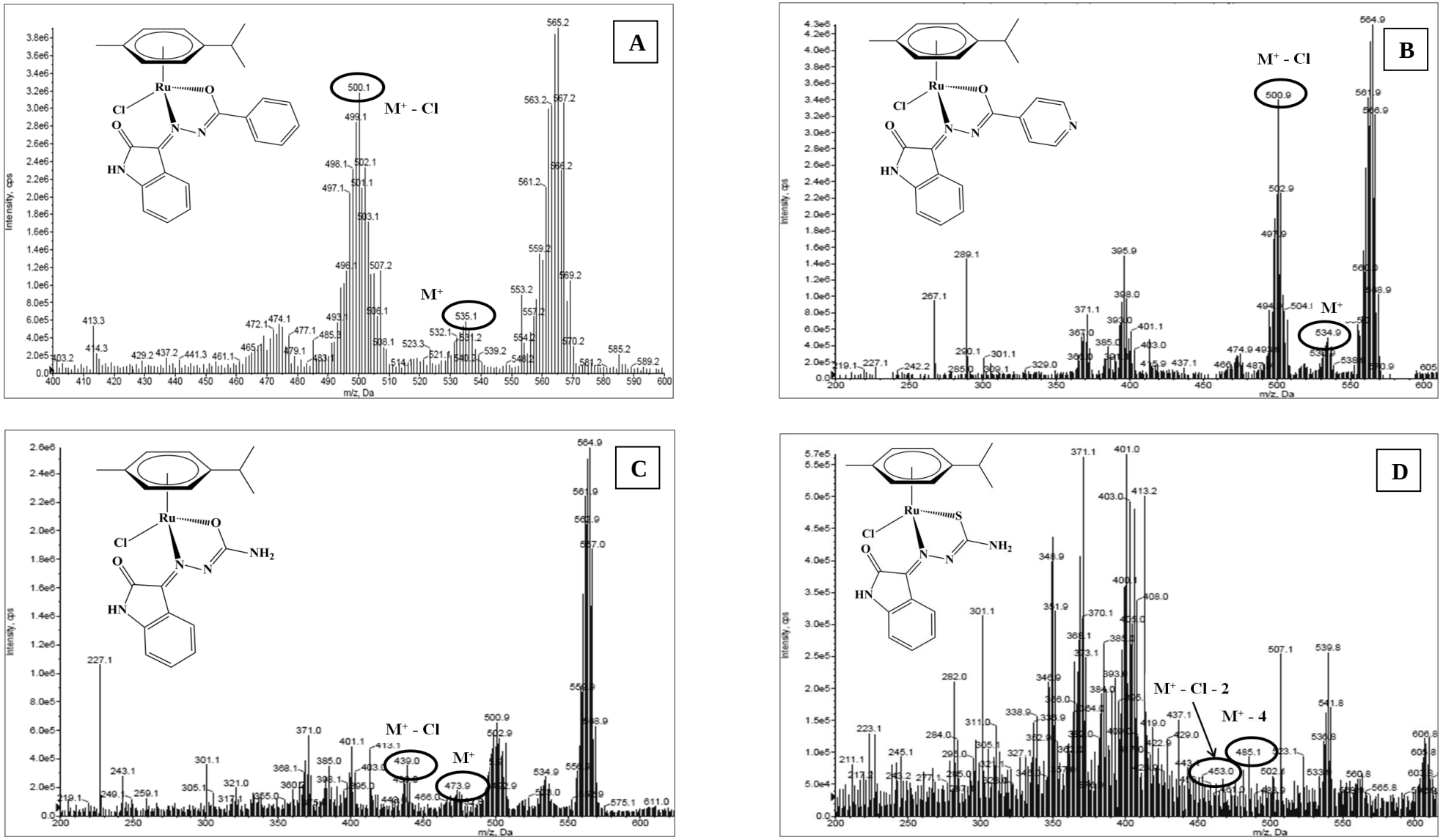

Fig. 4.14: *ESI-MS spectra of complexes (A)* ***RAIsa-1*** *(B)* ***RAIsa-2*** *(C)* ***RAIsa-3*** *(D)* ***RAIsa-4*** *indicating their molecular ion peak.*

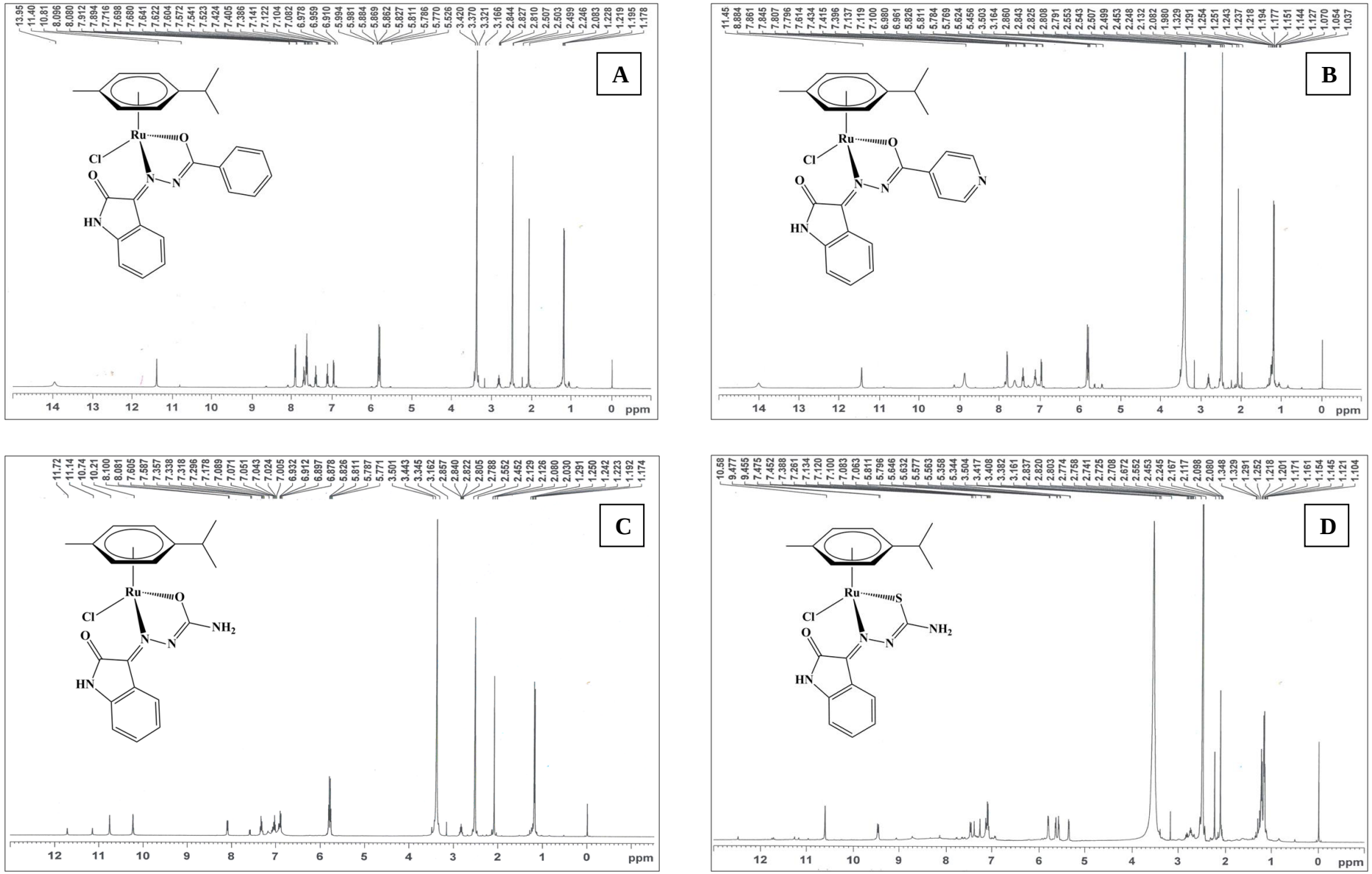

Fig. 4.15: *^{1}H NMR spectra of complexes (A)* ***RAIsa-1*** *(B)* ***RAIsa-2*** *(C)* ***RAIsa-3*** *(D)* ***RAIsa-4****.*

4.7 [Ru(η^6-p-cym)(Flq 1-3)Cl] complexes: (RAFlq 1-3)

4.7.1 Synthesis and characterization:

[Ru(η^6-p-cym)(Flq-1)Cl] **(RAFlq-1)**:

RAFlq-1 was synthesized by reaction of $[Ru(\eta^6\text{-}p\text{-cymene})Cl_2]_2$ (0.049 mmol, 30.0 mg) and ligand **Flq-1** (0.098 mmol, 34.6 mg). Soluble in almost all organic solvents like DMSO, MeOH, CH_2Cl_2. Yield: 56.1%; Molecular Weight 624.10 g/mole; Molecular Formula $C_{27}H_{35}ClF_2N_3O_3Ru$; Anal. Found: C, 49.58; H, 5.21; N, 6.38. Calc.: C, 51.96; H, 5.65; N, 6.73. ESI-MS *m/z*: 625.2 (M^++1), 588.2 (M^+-Cl); δ_H (400 MHz, DMSO-d_6) 5.82-5.77 (m, 4H, *p*-cym Ar-H), 2.85-2.79 (q, 1H, *p*-cym-*iso*-prop-CH), 2.08 (s, 3H, *p*-cym Ar-CH_3), 1.22 (d, 6H, *p*-cym-*iso*-prop-$(CH_3)_2$); FTIR (KBr/ cm^{-1}): $\nu_{(Ar)C\text{-}H}$ 2960, $\nu_{(pyridone)C=O}$ 1721, $\nu_{COOassym}$ 1623, ν_{COOsym} 1391, $\Delta\nu_{COO}$ 232.

[Ru(η^6-p-cym)(Flq-2)Cl] **(RAFlq-2)**:

RAFlq-2 was synthesized by reaction of $[Ru(\eta^6\text{-}p\text{-cymene})Cl_2]_2$ (0.049 mmol, 30.0 mg) and ligand **Flq-2** (0.098 mmol, 35.4 mg). Soluble in almost all organic solvents like DMSO, MeOH, CH_2Cl_2. Yield: 63.8%; Molecular Weight 632.11 g/mole; Molecular Formula $C_{28}H_{34}ClFN_3O_4Ru$; Anal. Found: C, 49.65; H, 5.22; N, 6.28. Calc.: C, 53.20; H, 5.42; N, 6.65. ESI-MS *m/z*: 634.2 (M^++2), 596.2 (M^+-Cl); δ_H (400 MHz, DMSO-d_6) 5.82-5.76 (m, 4H, *p*-cym Ar-H), 2.82-2.77 (q, 1H, *p*-cym-*iso*-prop-CH), 2.08 (s, 3H, *p*-cym Ar-CH_3), 1.19 (d, 6H, *p*-cym-*iso*-prop-$(CH_3)_2$); FTIR (KBr/ cm^{-1}): $\nu_{(Ar)C\text{-}H}$ 2959, $\nu_{(pyridone)C=O}$ 1713, $\nu_{COOassym}$ 1623, ν_{COOsym} 1337, $\Delta\nu_{COO}$ 286.

[Ru(η^6-p-cym)(Flq-3)Cl] **(RAFlq-3)**:

RAFlq-3 was synthesized by reaction of $[Ru(\eta^6\text{-}p\text{-cymene})Cl_2]_2$ (0.049 mmol, 30.0 mg) and ligand **Flq-3** (0.098 mmol, 32.4 mg). Soluble in almost all organic solvents like DMSO, MeOH, CH_2Cl_2. Yield: 59.4%; Molecular Weight 602.08 g/mole; Molecular Formula $C_{27}H_{32}ClFN_3O_3Ru$; Anal. Found: C, 50.09; H, 4.83; N, 6.51. Calc.: C, 53.86; H, 5.36; N, 6.98. ESI-MS *m/z*: 605.4 (M^++3), 567.2 (M^+-Cl); δ_H (400 MHz, DMSO-d_6) 5.82-5.76 (m, 4H, *p*-cym Ar-H), 2.83-2.77 (q, 1H, *p*-cym-*iso*-prop-CH), 2.08 (s, 3H, *p*-cym Ar-CH_3), 1.19 (d, 6H, *p*-cym-*iso*-prop-$(CH_3)_2$); FTIR (KBr/ cm^{-1}): $\nu_{(Ar)C\text{-}H}$ 2959, $\nu_{(pyridone)C=O}$ 1724, $\nu_{COOassym}$ 1629, ν_{COOsym} 1337, $\Delta\nu_{COO}$ 292.

4.7.2 Results and discussion:

In the IR spectra of all the three **RAFlq 1-3** complexes the stretching band of the free –COOH $\nu(C=O)_{carboxylate}$ at 1680-1700 cm^{-1} and ν(O-H) at 3420-3462 cm^{-1} found in the

ligands **Flq 1-3** has disappeared in Ru(II) coordinated fluoroquinolones. Two very strong characteristic bands appear in the range of 1620–1630 and 1330–1400 cm^{-1} assigned as ν(COO) asymmetric and symmetric stretching vibrations, respectively. The separation frequency $\Delta\nu = \nu(COO)_{asym} - \nu(COO)_{sym}$ values fall in the range 232–292 cm^{-1} indicating a monodentate coordination mode of the carboxylato group of the ligand [25, 27]. The band which should appear at ~1685 cm^{-1} for aromatic ketones assignable to free C=O stretching of the pyridone ring in the free fluoroquinolones has shifted to 1700-1725 cm^{-1} in the complexes suggesting the binding of fluoroquinolones to the metal centre through the pyridone carbonyl oxygen atom. Moreover the presence of weak to medium bands in the fingerprint regions 2900-3000 cm^{-1} owing to aromatic ν_{C-H} stretch and strong bands around 1430-1667 cm^{-1} due to the aromatic $\nu_{C=C}$ in plane vibrations is indicative of presence of *p*-cymene in the complex. The overall changes in the IR spectra suggest that all the three fluoroquinolones act as monoanionic bidentate ligand and interact with the metal center via the pyridone and carboxylate oxygen.

The electronic absorption spectra of the **RAFlq 1-3** complexes (*Fig. 4.16*) show three major bands in the wavelength range 200-400 nm. The first band appearing within 200-250 nm is attributable to the intraligand π→π* transition of the aromatic rings of the arene ligand (*p*-cymene) as well as the fluoroquinolone ligand. A second sharp but medium intensity peak is found in the range of 270-290 nm owing to the intraligand *n*→π* transitions which have blue shifted on complexation with the metal than those found in the free ligands. The third broad band observed within 325-335 nm is also due to the intraligand *n*→π* transitions which remains fairly unchanged. The λ_{max} values of all the transitions taking place in the complexes have been tabulated in *Table 4.10*.

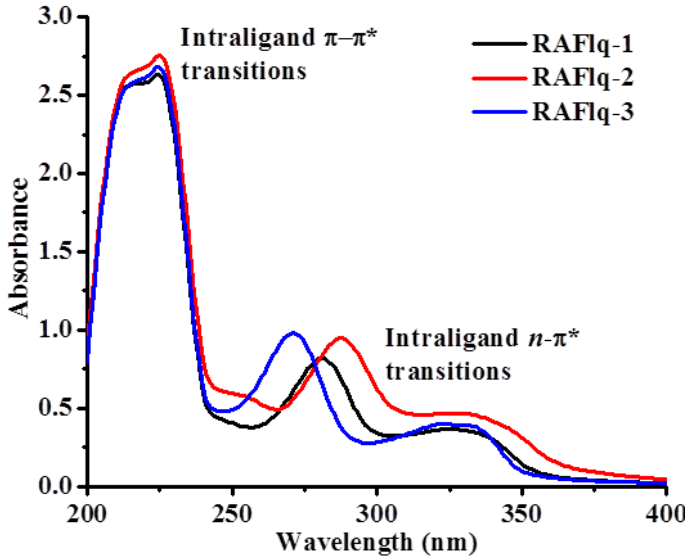

Fig. 4.16: *UV-vis. spectra of complexes* ***RAFlq 1-3*** *recorded in DMSO with path length 1 cm.*

Table 4.10: *UV-Vis. peak assignments of* ***RAFlq 1-3***

Compound	***Intra-ligand transitions (nm)***	
	π-π*	***n-π****
RAFlq-1	224	281, 328
RAFlq-2	225	288, 334
RAFlq-3	224	271, 329

The ESI-Mass spectra of **RAFlq 1-3** show *m/z* peaks corresponding to molecular ion M^+ as well as (M^+-Cl) values (*Table 4.11*). The *m/z* values of the molecular ion peaks for the complexes indicate that the *p*-cymene and one fluoroquinolone ligand (O, O donor) are coordinated to the metal centre. The mass spectra of all the complexes have been provided in *Fig. 4.17.*

Table 4.11: *m/z values of complexes* ***RAFlq 1-3****showing fragmentation.*

Compound	***m/z values***	***Fragments***
RAFlq-1	625.2	$[Ru(\eta^6\text{-}p\text{-cym})(Flq\text{-}1)Cl]^+$ +1 (M^++1)
	588.	$[Ru(\eta^6\text{-}p\text{-cym})(Flq\text{-}1)]^+$ (M^+-Cl)
RAFlq-2	634.2	$[Ru(\eta^6\text{-}p\text{-cym})(Flq\text{-}2)Cl]^+$ +2 (M^++2)
	596.2	$[Ru(\eta^6\text{-}p\text{-cym})(Flq\text{-}2)]^+$ (M^+-Cl)
RAFlq-3	605.4	$[Ru(\eta^6\text{-}p\text{-cym})(Flq\text{-}3)Cl]^+$ +3 (M^++3)
	567.2	$[Ru(\eta^6\text{-}p\text{-cym})(Flq\text{-}3)]^+$ (M^+-Cl)

The ^{1}H NMR spectra of **RAFlq 1-3** (*Fig. 4.18*) show distinct peaks corresponding to *p*-cymene observed at the same δ values as discussed in *sec. 4.3.2*. Rest of the peaks are associated with the fluoroquinolone ligand. The peak arising due to carboxylic O-H proton in the free ligands is no longer seen in the spectra of the complexes indicating coordination of the carboxylate oxygen to the ruthenium metal center. Moreover the peaks owing to the aromatic protons of the quinolone nucleus are observed in the region δ = 7-9 ppm while those arising due to piperazine protons are obtained in the region δ = 3-4 ppm. The methyl and substituted methyl protons appear at around δ = 1-2 ppm.

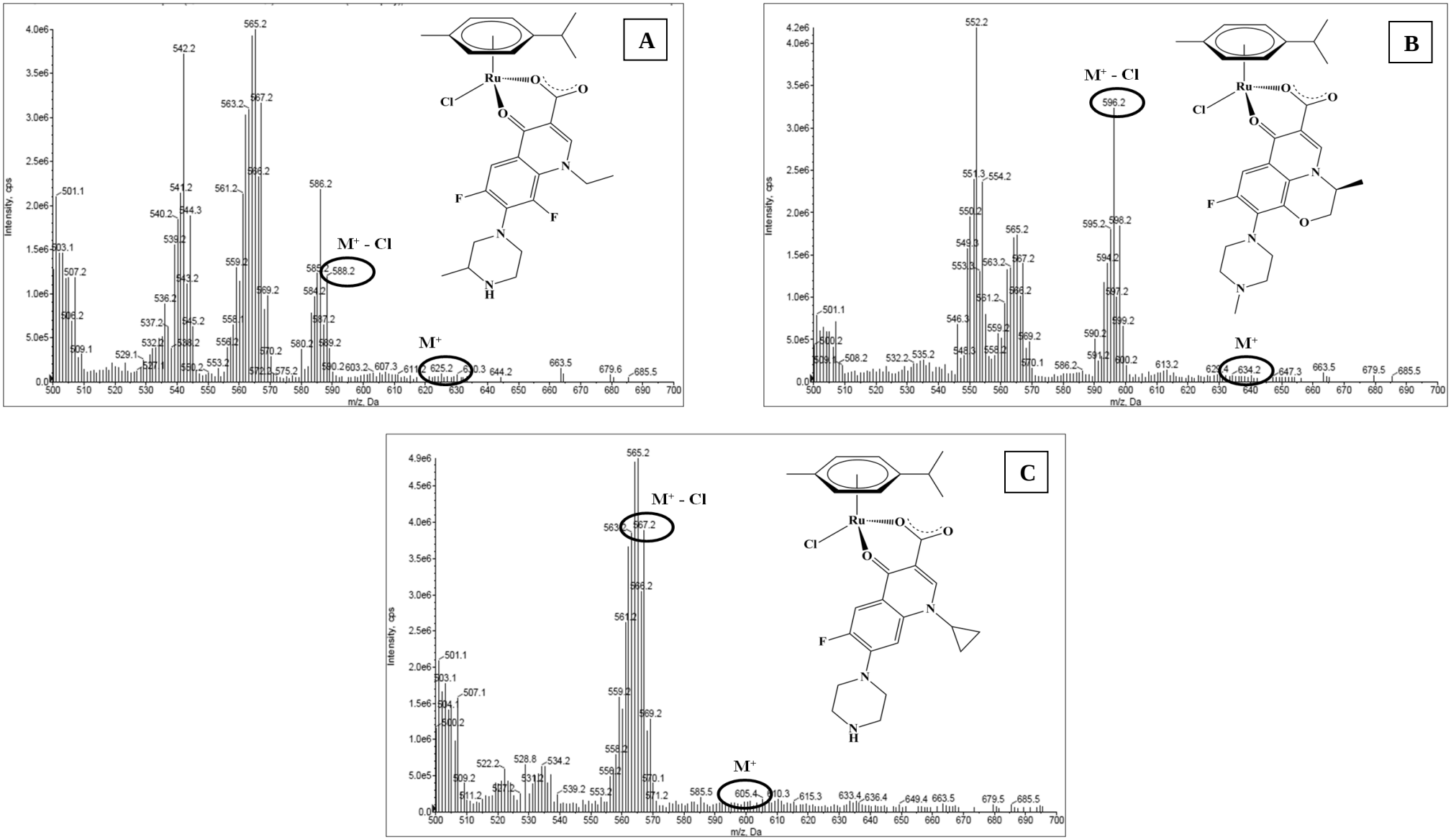

Fig. 4.17: *ESI-MS spectra of complexes (A)* ***RAFlq-1*** *(B)* ***RAFlq-2*** *(C)* ***RAFlq-3*** *indicating their molecular ion peak.*

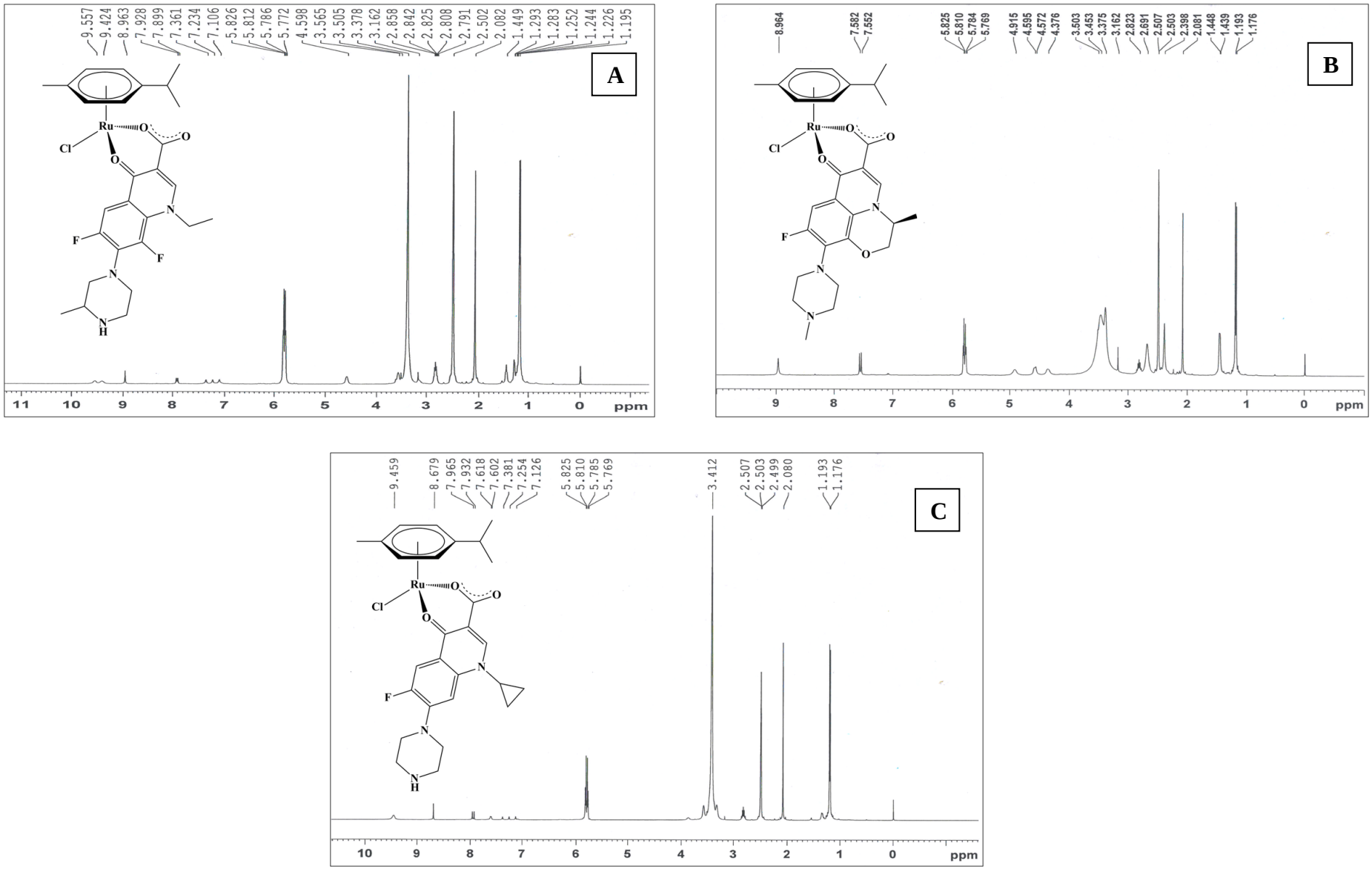

Fig. 4.18: *^{1}H NMR spectra of complexes (A)* ***RAFlq-1*** *(B)* ***RAFlq-2*** *(C)* ***RAFlq-3***

4.8 Summary:

The five different [Ru(*p*-cym)(L)Cl] complex series discussed in this chapter have been synthesized and well characterized with an aim to evaluate them for their biomolecular interactions and *in cellulo* anticancer activities.

4.9 References:

[1] Jaouen, G.; Vessieres, A. *Pure Appl. Chem.*, **1985**, *57*, 1865.

[2] Randaccio, L.; Furlan, M.; Geremia, S.; Slouf, M.; Srnova, I.; Toffoli, D. *Inorg. Chem.*, **2000**, *39*, 3403.

[3] Top, S.; Jaouen, G.; Vessieres, A.; Abjean, J. P.; Davoust, D.; Rodger, C. A.; Sayer, B. G.; McGlinchey, M .J. *Organometallics*, **1985**, *4*, 2143.

[4] Allardyce, C. S.; Dorcier, A.; Scolaro, C.; Dyson, P. J. *Appl. Organomet. Chem.*, **2005**, *19*, 1.

[5] Hartinger, C. G.; Zorbas-Seifried, S.; Jakupec, M. A.; Kynast, B.; Zorbas, H.; Keppler, B. K. *J. Inorg. Biochem.*, **2006**, *100*, 891.

[6] Hartinger, C. G.; Jakupec, M. A.; Zorbas-Seifried, S.; Groessl, M.; Egger, A.; Berger, W.; Zorbas, H.; Dyson, P. J.; Keppler, B. K. *Chem. Biodivers.*, **2008**, *5*, 2140.

[7] Pacor, S.; Zorzet, S.; Cocchietto, M.; Bacac, M.; Vadori, M.; Turrin, C.; Gava, B.; Castellarin, A.; Sava, G. *J. Pharmacol. Exp. Ther.*, **2004**, *310*, 737.

[8] Sava, G.; Zorzet, S.; Turrin, C.; Vita, F.; Soranzo, M.; Zabucchi, G.; Cocchietto, M.; Bergamo, A.; DiGiovine, S.; Pezzoni, G.; Sartor, L.; Garbisa, S. *Clin. Cancer Res.*, **2003**, *9*, 1898.

[9] Dougan, S. J.; Melchart, M.; Habtemariam, A.; Parsons, S.; Sadler, P. J. *Inorg. Chem.*, **2006**, *45*, 10882.

[10] Wang, F.; Habtemariam, A.; van der Geer, E. P. L.; Fernandez, R.; Melchart, M.; Deeth, R. J.; Aird, R.; Guichard, S.; Fabbiani, F. P. A.; Lozano-Casal, P.; Oswald, I. D. H.; Jodrell, D. I.; Parsons, S.; Sadler, P. J. *Proc. Natl. Acad. Sci. U.S.A.*, **2005**, *102*, 18269.

[11] Pizarro, A. M.; Abraha, H.; Sadler, P. J. *Top. Organomet. Chem.*, **2010**, *32*, 21.

[12] Yaw, K. Y.; Michael, M.; Abraha, H.; Sadler, P. J. *Chem. Commun.*, **2005**, 4764.

[13] Dyson, P. J. *Chimia*, **2007**, *61*, 698.

[14] Dougan, S. J.; Sadler, P. J. *Chimia*, **2007**, *61*, 704.

[15] Dale, L. D.; Tocher, J. H.; Dyson, T. M.; Edwards, D. I.; Tocher, A. *Anti-Cancer Drug Design*, **1992**, ***7***, 3.

[16] Allardyce, C. S.; Dyson, P. J.; Ellis, D. J.; Heath, S. L. *Chem. Commun.*, **2001**, 1396.

[17] Morris, R. E.; Aird, R. E.; Murdoch, P. d. S.; Chen, H.; Cummings, J.; Hughes, N. D.; Pearsons, S.; Parkin, A.; Boyd, G.; Jodrell, D. I.; Sadler, P. J. *J. Med. Chem.*, **2001**, *44*, 3616.

[18] Alexey, A. N.; Hartinger, C. G.; Dyson, P. J. *J. Organomet. Chem.*, **2014**, *751*, 251.

[19] Bennett, M. A.; Smith, A. K. *J. Chem. Soc., Dalton Trans.*, **1974**, 233.

[20] Tönnemann, J.; Risse, J.; Grote, Z.; Scopelliti, R.; Severin, K. *Eur. J. Inorg. Chem.*, **2013**, *2013*, 4558.

[21] Suss-Fink, G. *Dalton Trans.*, **2010**, *39*, 1673.

[22] Bennett, M. A.; Huang, T. N.; Matheson, T. W.; Smith, A. K. *Inorg. Synth.*, **1982**, *21*, 74.

[23] Manimaran, A.; Prabhakaran, R.; Deepa, T.; Natarajan, K.; Jayabalakrishnan, C. *Appl. Organometal. Chem.*, **2008**, *22*, 353.

[24] Bottari, B.; Maccari, R.; Monforte, F.; Ottana, R.; Rotondo, E.; Vigorita, M. G. *Bioorg. Med. Chem. Lett.*, **2001**, *11*, 301.

[25] Deacon, G. B.; Phillips, R. *J. Coord. Chem. Rev.*, **1980**, *33*, 227.

[26] Gehad, G.; Mohamed, H. F.; El-Halim A.; Maher, M. I.; El-Dessouky, W.; Mahmoud, H. *J. Mol. Struct.*, **2011**, *999*, 29.

[27] Turel, I. *Coord. Chem. Rev.*, **2002**, *232*(1-2), 27.